RESEARCH ARTICLE

Conserved Senescence Associated Genes and Pathways in Primary Human Fibroblasts Detected by RNA-Seq

S. Marthandan[1]*, M. Baumgart[1], S. Priebe[2], M. Groth[1], J. Schaer[2], C. Kaether[1], R. Guthke[2], A. Cellerino[1,3], M. Platzer[1], S. Diekmann[1], P. Hemmerich[1]

1 Leibniz-Institute on Aging—Fritz Lipmann Institute e.V. (FLI), Jena, Germany, **2** Leibniz Institute for Natural Product Research and Infection Biology—Hans-Knöll-Institute e.V. (HKI), Jena, Germany, **3** Laboratory of NeuroBiology, Scuola Normale Superiore, Pisa, Italy

* smarthandan@fli-leibniz.de

Abstract

Cellular senescence correlates with changes in the transcriptome. To obtain a complete view on senescence-associated transcription networks and pathways, we assessed by deep RNA sequencing the transcriptomes of five of the most commonly used laboratory strains of human fibroblasts during their transition into senescence. In a number of cases, we verified the RNA-seq data by real-time PCR. By determining cellular protein levels we observed that the age-related expression of most but not all genes is regulated at the transcriptional level. We found that 78% of the age-affected differentially expressed genes were commonly regulated in the same direction (either up- or down-regulated) in all five fibroblast strains, indicating a strong conservation of age-associated changes in the transcriptome. KEGG pathway analyses confirmed up-regulation of the senescence-associated secretory phenotype and down-regulation of DNA synthesis/repair and most cell cycle pathways common in all five cell strains. Newly identified senescence-induced pathways include up-regulation of endocytotic/phagocytic pathways and down-regulation of the mRNA metabolism and the mRNA splicing pathways. Our results provide an unprecedented comprehensive and deep view into the individual and common transcriptome and pathway changes during the transition into of senescence of five human fibroblast cell strains.

Introduction

Normal human fibroblasts have a finite proliferative capacity in culture, a phenomenon termed "senescence" [1, 2]. Senescent cells remain metabolically active but exit the cell cycle and stop proliferating, resulting in a decreased incidence of cancer. *In vivo*, senescence may enable removal of damaged cells and support tissue remodeling by cell cycle arrest, induction of a secretory pathway which recruits immune cells, and by recruiting progenitor cells to re-populate the tissue [3]. Furthermore, senescent cells are involved in *in vivo* aging due to their adverse impact on function and renewal of stem cells [4]. Most importantly, senescent cells that

Abbreviations: CDKIs, Cyclin-dependent kinase inhibitors; SA, β galactosidase–Senescence associated β- galactosidase activity; TIF, Telomere dysfunction-induced foci; SAHF, Senescence associated heterochromatin foci; SASP, Senescence-associated secretory phenotype; PD, Population doublings; pRB, Phosphorylated retinoblastoma protein; HFF, Human foreskin fibroblast; DMEM, Dulbeccos modified Eagles low glucose medium; FBS, Fetal bovine serum; PBS, Phosphate buffered saline; rSFRP4, recombinant secreted frizzled-related protein 4; DKK3, Dickkopf-related protein 3; RT, Room temperature; DAPI, 4'-6-diamidine-2-phenyl indole; GAPDH, Glyceraldehyde 3-phosphate dehydrogenase; ACTB, Beta-actin; RAB10, Ras-related protein 10; RNA-seq, High-throughput RNA sequencing; RIN, RNA integrity number; RPKM, Reads Per Kilobase of transcript per Million mapped reads; MDS plots, Multi-dimensional scaling plots; DEG, Differentially expressed genes; GEO, Gene Expression Omnibus; HDF, Human dermal fibroblasts; KEGG pathways, Kyoto Encyclopedia of Genes and Genomes; CTSK, Cathepsin K; TMEM47, Transmembrane protein 47; CCNB1, Cyclin B1; CCNA2, Cyclin A2; C3, Complement 3; Wnt-16, Protein Wnt-16; IGFBP2, Insulin-like growth factor-binding protein 2; CCND1, Cyclin D1; p21, Cyclin-dependent kinase inhibitor 1 (CDKN1A); IGFBP3, Insulin-like growth factor-binding protein 3; IGFBP5, Insulin-like growth factor-binding protein 5; HAS2, Hyaluronan synthase 2; KIF20A, Kinesin-like protein KIF20A; KIF11, Kinesin family member 11; CCNB2, Cyclin B2; ANLN, Annilin; TOP2A, DNA topoisomerase 2-alpha; RRM2B, Ribonucleoside-diphosphate reductase subunit M2 B; HEXB, Beta-hexosaminidase subunit beta; AKR1B1, Aldo-keto reductase family 1, member B1 (aldose reductase); SMPD1, Sphingomyelin phosphodiesterase 1; PEA15, Astrocytic phosphoprotein; DYNLT3, Dynein, light chain, Tctex-type 3; MOAP1, Modulator of apoptosis 1; SERINC3, Serine incorporator 3; NPC2, Niemann–Pick type C; ZMAT3, zinc finger matrin-type 3; TNFRSF10D, Tumor Necrosis Factor Receptor Superfamily, Member 10d; LRP10, Low Density Lipoprotein Receptor-Related Protein 10; MCM6, Minichromosome Maintenance Complex Component 6; CDC6, Cell division cycle 6; SET, SET Nuclear Proto-Oncogene; RAD21, RAD21 Homolog, Nuclear Matrix Protein 1; AXL, Receptor Tyrosine kinase; HNRPM, Heterogeneous Nuclear Ribonucleoprotein M; SNRPD1, Small Nuclear Ribonucleoprotein D1 Polypeptide; HIST1H1C, Histone Cluster 1, H1c;

accumulate during adulthood in mice negatively influence lifespan and promote age-dependent changes in several organs [5].

Some of the major factors responsible for cellular senescence include DNA damage [6–8], oxidative stress [9, 10] and other factors [6, 11–14], resulting in an induction of cyclin-dependent kinase inhibitors (CDKIs) [15]. In spite of the lack of a single specific marker for cellular senescence, there are several cell specific markers *in vitro* and *in vivo* [16–19]: increased cell size associated with high number of lysosomes, vacuoles and mitochondria, cytoskeletal changes [20], senescence associated increase in βgalactosidase activity (SA-β Gal) [16], telomere dysfunction-induced foci (TIF) [21, 22], up-regulation of specific cell cycle regulators [23, 24], development of senescence associated heterochromatin foci (SAHF) [17, 25], altered expression pattern of genes [26, 27], secretion of proteins associated with senescence-associated secretory phenotype (SASP) [28–31] and accumulation of Annexin V at the nuclear envelope [32]. Senescent cells, despite their viability and active metabolism, have been demonstrated to be resistant to mitogenic or apoptotic stimuli [33–35].

Several mechanisms and pathways, mainly the p53-p21 and p16-pRB axes, and telomere shortening have been well documented as cellular senescence inducers [2, 18, 21, 22, 36–46]. Human fibroblasts have been routinely used to study cellular senescence [4, 28, 47, 48]. The ability of human fibroblasts to undertake a limited number of population doublings (PDs) varying from 50 to 80, depending on fibroblast cell type, until they reach a state of permanent cell cycle arrest (called "Hayflick limit") make them an ideal model system for investigating cellular aging [1]. Cellular senescence of some types of primary mammalian cells in culture partly mirrors the mechanisms of aging *in vivo* [4, 49]. The aim of this investigation was to identify genes and pathways associated with cellular senescence by assessing the transcriptomes of five different human fibroblast strains during *in vitro* aging. We found a strong conservation of age-associated changes in the transcriptome of these five cell strains with only a minor strain-specific contribution.

Materials and Methods

Cell strains

Primary human fibroblasts MRC-5 (14 weeks gestation male, fibroblasts from normal lung, normal diploid karyotype), WI-38 (3 months gestation female, fibroblasts from normal lung, normal diploid karyotype), BJ (newborn male, fibroblasts from normal foreskin, normal diploid karyotype) and IMR-90 (fibroblasts from 16 weeks female fetus, lung, normal diploid karyotype) were obtained from ATCC (LGC Standards GmbH, Wesel, Germany). HFF (primary cells, *Homo sapiens*, fibroblasts from foreskin, normal diploid karyotype) cells were kind gifts of T. Stammiger (University of Erlangen, [50]).

Cell culture

Cells were cultured as recommended by ATCC in Dulbeccos modified Eagles low glucose medium (DMEM) with L-glutamine (PAA Laboratories, Pasching, Austria), supplemented with 10% fetal bovine serum (FBS) (PAA Laboratories). Cells were grown under normal air conditions in a 9.5% CO_2 atmosphere at 37°C. For sub-culturing, the remaining medium was discarded and cells were washed in 1 x PBS (pH 7.4) (PAA Laboratories) and detached using trypsin/EDTA (PAA Laboratories). Primary fibroblasts were sub-cultured in a 1:4 (= 2 population doublings (PDs)) or 1:2 (= 1 PD) ratio. For stock purposes, cryo-conservation of the cell strains at various PDs were undertaken in cryo-conserving medium (DMEM + 10% FBS + 5% DMSO). Cells were immediately frozen at -80°C and stored for two to three days. Afterwards,

UBE2T, Ubiquitin-Conjugating Enzyme E2T; TPX2, Targeting protein for Xklp2; RNASEH2A, Ribonuclease H2, Subunit A; CDC20, Cell division cycle 20; TK1, Thymidine kinase 1; CEP55, Centrosomal Protein 55kDa; HMGB2, High Mobility Group Box 2; RRM2, Ribonucleotide Reductase M2; CENPW, Centromere protein W; KIFC1, Kinesin Family Member C1; GAGE, Generally Applicable Gene-set Enrichment; p16, Cyclin-Dependent Kinase Inhibitor 2A; p15, Cyclin-Dependent Kinase Inhibitor 2B; p27, Cyclin-Dependent Kinase Inhibitor 1B; MMPs, Matrix metallopeptidase; FOXM1, Forkhead Box M1; CENPF, Centromere Protein F; MEFs, Mouse embryonic fibroblasts; E2F1, E2F Transcription Factor 1; PAI-1, Plasminogen activator inhibitor; ATF1, Activating transcription factor 1; HSF1, Heat Shock Transcription Factor 1; CREB1, CAMP Responsive Element Binding Protein 1; h, hours; NFκB1, NF kappa B signaling; wt, Wild type; IRS-1, Insulin receptor substrate 1.

cells were transferred to liquid nitrogen for long time storage. Re-freezing and re-thawing was not performed to avoid premature senescence [51].

One vial of each of the five different fibroblast cell strains (MRC-5, HFF, BJ, WI-38 and IMR-90) were obtained and maintained in culture from an early PD. On obtaining enough stock on confluent growth of the fibroblasts in 75 cm^2 flasks, cells were sub-cultured into three separate 75 cm^2 flasks ("triplicates") and were passaged until they were senescent in culture (Fig 1A).

Treatment of human fibroblasts with recombinant human proteins

HFF (PD = 18), BJ (PD = 34) and MRC-5 (PD = 32) fibroblasts of early PD were maintained in conditioned DMEM medium containing different concentrations (0, 5, 10, 15, 25, 30 μg/ml) of recombinant SFRP4 (rSFRP4; 1827-SF-025; R&D SYSTEMS). SFRP4 containing medium was replenished every 2 days. A similar procedure was undertaken in HFF strains (PD = 22) with rDKK3 (1118-DK-050; R&D SYSTEMS) for a range of concentrations (0, 0.1, 1, 10, 50 μg/ml). The samples were analyzed at different time points (0, 2, 6, 10 days) for the induction of senescence using SA-β galactosidase assay (SA-β Gal) and typical senescence markers in immunoblotting.

RNA interference and transfection method

HFF cells were transiently transfected with a range of concentrations (0–150 nM) of siRNA against SFRP4 (FlexiTube GeneSolution GS20379; Qiagen, Germany), using Lipofectamine 2000 (11668–019; Life Technologies, Invitrogen, Germany). Specific gene knock down was evaluated by immunoblotting.

Detection of SA-β galactosidase activity

The SA-β Gal assay was performed as described by [16] in each of the five fibroblast cell strains at the frequency of every four PDs from early PDs until they were senescent (late PDs). Cells were washed in 1xPBS (pH 7.4) and fixed in 4% paraformaldehyde (pH 7.4), 10 min at room temperature (RT). After washing the cells in 1xPBS (pH 7.4), staining solution consisting of 1 mg/ml X-Gal, 8 mM citric acid /sodium phosphate pH 6,0, 5 mM $K_3Fe(CN)_6$, 5 mM $K_4Fe(CN)_6$, 150 mM NaCl, 2 mM $MgCl_2$, was added. The enzymatic reaction occurred without CO_2 for 4–16 h at 37°C. After incubation, the cells were washed in 1xPBS (pH 7.4) and, in order to visualize cell nuclei, DNA and SAHFs, mounted with 4'-6-diamidine-2-phenyl indole (DAPI) containing Prolong Gold antifade reagent (Invitrogen). Paired two-sample type 2 Student's t-tests assuming equal variances were done to examine the values obtained from SA-β Gal assay for statistical significance.

Immunoblotting

For immunoblotting, 10,000 cells/μl were used. Immunodetection was performed using 5%-powdered milk in PBS-T (1xPBS, pH 7.4 and 1% Tween 20) for blocking (Roth, Germany). The optimal concentration of all the primary antibodies was estimated in human fibroblasts. Primary antibodies, anti-p21 mouse antibody (OP64; Calbiochem; dilution 1:200), anti-p15 rabbit antibody (4822; Cell Signaling Technology; 1:250), anti-p16 mouse antibody (550834; BD Pharmingen; 1:200), anti-p27 rabbit antibody (sc-528; Santa Cruz; 1:200), anti-Anillin rabbit antibody (ANLN; ab99352; Abcam; 1:2000), anti-HSPC150 rabbit antibody (UBE2T; ab110459; Abcam; 1:500), anti-RNASEH2A mouse antibody (WH0010535M1; SIGMA-Aldrich; 1:500), anti-TPX2 rabbit antibody (ab71816; Abcam; 1:100), anti-KIF20A rabbit
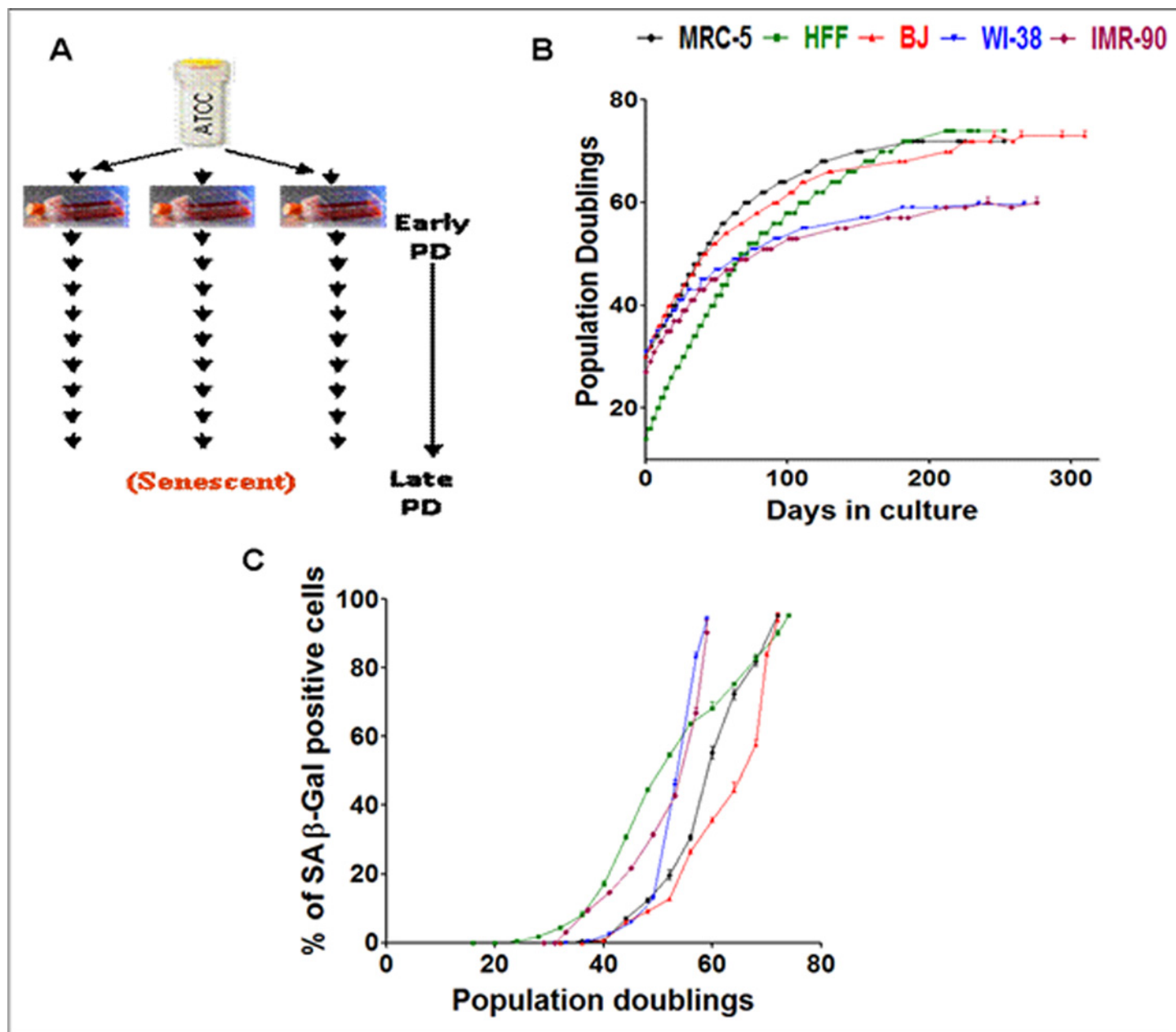
Fig 1. Experimental design, growth curves and transition into senescence. (A) Experimental plan of culturing fibroblast cell strains derived from a single vial and maintained in culture as triplicates from an early PD until senescence at late PDs. (B) Growth curve of five different fibroblast cell strains (MRC-5, BJ, WI-38, IMR-90, HFF) derived from a single vial and maintained in culture as triplicates from an early PD until senescence at late PDs. Data points of all measurements are displayed (not the mean). (C) Percentage of SA-β Gal positive cells at different time points of their growth in culture in the five fibroblast strains derived from a single vial. Each curve is measured in triplicate, the mean value is displayed with error bar (± S.E).

antibody (ab85644; Abcam; 1:500), anti-KIFC1 rabbit antibody (ab172620; Abcam; 1:15000), anti-CENPW rabbit antibody (PA5-34441; Thermo Scientific; 1:100), anti-RRM2 mouse antibody (ab57653; Abcam; 1:100), anti-HMGB2 rabbit antibody (ab11973; Abcam; 1:500), anti-Thymidine Kinase 1 rabbit antibody (TK1; ab76495; Abcam; 1:5000), anti-Cyclin B2 rabbit antibody (CCNB2; ab82287; rabbit; 1:100), anti-CEP55 rabbit antibody (ab84580; Abcam; 1:1000), anti-Cyclin B1 mouse antibody (CCNB1; ab72; Abcam; 1:1000), anti-Eg5 rabbit

antibody (KIF11; ab61199; Abcam; 1:500), anti-Topoisomerase II alpha rabbit antibody (TOP2A; ab74715; Abcam; 1:500), anti-CDC20 rabbit antibody (ab26483; Abcam; 1:100), anti-Histone H1.2 rabbit antibody (HIST1H1C; ab17677; Abcam; 1:1000), anti-p53R2 rabbit antibody (RRM2B; ab8105; Abcam; 1:500), anti-Dkk3 goat antibody (ab2459; Abcam; 1:5000), anti-TMEM47 rabbit antibody (SAB1104840; SIGMA-Aldrich; 1:250), anti-SFRP4 rabbit antibody (ab154167; Abcam; 1:1000), anti-beta Catenin rabbit antibody (ab16051; Abcam; 1:2500) and anti-tubulin mouse antibody (T-9026; SIGMA-Aldrich; 1:5000) were diluted in 5%-powdered milk (in PBS-T) and incubated for 1 h at RT. Washing steps were performed 3×10 min in 1×PBS-T. The secondary horseradish peroxidase-labeled antibodies (Jackson Immuno Research Lab) were incubated for 1 h at RT. Detection of horseradish peroxidase was performed using ECL-detection system and radiographic film (GE Healthcare, Germany). After film development, signal intensities of immunoblot bands were quantified using Metamorph software [52]. The signal intensity values were examined for statistical significance using paired two-sample type 2 Student's t-tests assuming equal variances.

RNA extraction

Total RNA was isolated using Qiazol (Qiagen, Hilden, Germany) according to the manufacturer's protocol, with modifications. In brief, the fibroblasts were pelleted in 2 ml safe-lock tubes (Eppendorf, Hamburg, Germany). 1 ml cooled Qiazol and one 5 mm stainless steel bead (Qiagen) were added. Homogenization was performed using a TissueLyzer II (Qiagen) at 20 Hz for 1 min. After incubation for 5 min at RT, 200 ml chloroform was added. The tube was shaken for 15 sec and incubated for 3 min at RT. Phase separation was achieved by centrifugation at 12,000 x g for 20 min at 4°C. The aqueous phase was transferred into a fresh cup and 10 mg of glycogen (Invitrogen, Darmstadt, Germany), 0.16 volume NaOAc (2 M, pH 4.0) and 1.1 volume isopropanol were added, mixed and incubated for 10 min at RT. The RNA was precipitated by centrifugation with 12,000 x g at 4°C for 20 min. The supernatant was removed and the pellet was washed with 80% ethanol twice and air dried for 10 min. The RNA was re-suspended in 20 µl DEPC-treated water by pipetting up and down, followed by incubation at 65°C for 5 min. The RNA was quantified with a NanoDrop 1000 (PeqLab, Erlangen, Germany) and stored at -80°C until use.

Quantitative real-time PCR

Real-time PCR was performed by use of CFX384 thermocycler (Biorad, München, Germany) and Quantitect PCR system (Qiagen). Steps were processed as recommended by the manufacturer. We used 500 ng total RNA for cDNA synthesis in a 20 µl volume. After cDNA synthesis samples were diluted to a final volume of 200 µl with ultra-pure water. PCR reactions were performed in 10 µl volume with 2 µl diluted cDNA using the Quantitect SYBR Green PCR kit (Qiagen). A cDNA pool was serially diluted in steps of 1:1 (from 80 to 2.5 ng per reaction) and used to create standard as well as melting curves and to calculate amplification efficiencies for each primer pair prior to use for quantification. Primers are listed in S1 Table. All reactions were performed in triplicates and negative (water) as well as genomic (without reverse transcriptase) controls were always included. Fold changes describe the difference in expression level between old and young PDs normalized to three reference genes GAPDH, ACTB, and RAB10. RAB10 was selected as reference gene, since, based on our RNA sequencing (RNA-seq) results, its expression was stable through all cell strains and PDs. Statistical analysis of real-time data was performed with the relative expression software tool REST (Qiagen; [53]). This software tool uses a mathematical model which compares unknown and control samples, and calculates the significance of the differences by a pairwise fixed reallocation randomization test.

RNA-seq

For quality check, total RNA was analyzed using Agilent Bioanalyzer 2100 (Agilent Technologies) and RNA 6000 Nano Kit (Agilent) to ensure appropriate RNA quality in terms of degradation (average RNA integrity number (RIN) of 8). Total RNA was used for Illumina library preparation and RNA-seq [54]. 2.5 µg total RNA was used for indexed library preparation using Illumina's TruSeq RNA Sample Prep Kit v2 following the manufacturer's instruction. Libraries were pooled and sequenced (5 samples per lane) using a HiSeq2000 (Illumina) in single read mode with 50 cycles using sequencing chemistry v3. Sequencing resulted in approximately 40 million reads with a length of 50 bp (base pairs) per sample. Reads were extracted in FastQ format using CASAVA v1.8.2 or v1.8.3 (Illumina).

RNA-seq data analysis

Raw sequencing data were received in FASTQ format. Read mapping was performed using Tophat 2.0.6 [55] and the human genome references assembly GRCh37 (http://feb2012. archive.ensembl.org/). The resulting SAM alignment files were processed using the HTSeq Python framework and the respective GTF gene annotation, obtained from the Ensembl database [56]. Gene counts were further processed using the R programming language [57] and normalized to Reads Per Kilobase of transcript per Million mapped reads (RPKM) values. In order to examine the variance and the relationship of global gene expression across the samples, different correlation values have been computed including Spearman's correlation of gene counts and Pearson's correlation of log2 RPKM values. The resulting correlation values were visualized using multi-dimensional scaling plots (MDS) and heatmaps (S2 Fig).

Subsequently, the Bioconductor packages DESeq [58] and edgeR [59] were used to identify differentially expressed genes (DEG). Both packages provide statistics for determination of differential expression in digital gene expression data using a model based on the negative binomial distribution. The non-normalized gene counts have been used here, since both packages include internal normalization procedures. The resulting p-values were adjusted using the Benjamini and Hochberg's approach for controlling the false discovery rate (FDR) [60]. Genes with an adjusted p-value < 0.05 found by both packages were assigned as differentially expressed.

Examination of the correlation between the samples

After mapping, counting and normalization of the RNA-seq data, Spearman's correlation was computed for each pair of samples using the expression values of all expressed genes. The resulting correlation values were visualized using Heatmap plots (S2 Fig). A similar approach had been described by [61] (S1 Fig) where the replicates exhibited high correlation since these values resulted from the re-sequencing of the same library. By this approach we determine the experimental error of our approach.

Analysis of public data sets (previously published scientific literature on age related studies in human fibroblasts)

In order to compare our expression data of the five fibroblast cell strains with previously published gene expression data sets, we searched the Gene Expression Omnibus (GEO, http://www.ncbi.nlm.nih.gov/geo/) repository [62], the ArrayExpress Archive (http://www.ebi.ac.uk/arrayexpress; [63]) and in PubMed for studies including replicative senescence in human fibroblasts. Altogether, we found 8 studies where raw data files were available. In some cases, only a subset of all available samples was used (as indicated).

1. [64] Two-color microarray data was downloaded from GEO (GSE4352). The following samples were used: GSM85982, GSM85986, GSM85989, GSM85977, GSM85979, GSM85978, GSM85983. Early passage proliferating cells (BJ, WS1, WI-38) were compared with senescent cells.

2. [65] Two-color microarray data including two replicates was received upon request from the authors. Young and old human dermal fibroblasts (HDF) were compared.

3. [66] Two-color microarray data was downloaded from GEO (GSE687). All 16 samples from four different cell strains (human mammary stroma) were used. Proliferating cells were compared with senescent cells.

4. [67] Two-color microarray data was downloaded from GEO (GSE6762). The following samples were used: GSM155829, GSM155830, GSM155831, GSM155832. Proliferating was compared to senescent HFF strains.

5. [68] Two-color microarray data was downloaded from GEO (GSE15919). The following samples were used: GSM399555, GSM399560, GSM399561, GSM399569, GSM399571, GSM399581. Young and senescent MRC-5 fibroblasts were compared.

6. [69] Affymetrix microarray data was downloaded from GEO (GSE19018). All 12 samples were used which included young, old and senescent IMR-90 cells under either 3% or 20% oxygen (O_2). Both O_2 levels were analyzed independently resulting in two data sets for this study.

7. [70] Illumina Beadchip expression data was downloaded from GEO (GSE41714). This data set comprises of 12 samples from HDFs including a set of different PDs. We compared samples GSM1023041, GSM1023042, GSM1023043, GSM1023044 (early PD) with GSM1023050, GSM1023051, GSM1023052 (late PD).

8. [71] Affymetrix microarray data was downloaded from ArrayExpress (E-MTAB-2086). We compared IMR-90 samples DL10041401, DL10082501, DL10082502 (young) with DL10082507, DL10082508 (senescent).

The processing of the microarray raw data [69; 71] derived from different measurements was performed using the statistical programming language R and several R packages. The 2-color microarray [64–68] and Illumina Beadchip [70] data sets were analyzed using *GEOquery* [72], and *limma* [73]. Affymetrix microarrays [69, 71] were analyzed using *affy* [74] and custom chip-definition files downloaded from Brainarray (brainarray.mbni.med.umich.edu). Background correction, normalization, calculation of log2 fold-changes and identification of DEG was performed using *limma*. The resulting p-values were adjusted using the Benjamini and Hochberg's approach for controlling FDR. In order to compare all data sets, gene IDs had to be converted between various formats depending on the measurement platform. We used the Ensembl database (http://www.ensembl.org/biomart/martview/) and bioDBnet (http://biodbnet.abcc.ncifcrf.gov/) as well as our own mapping pipelines.

Retrieval of genes most significantly differentially regulated with age commonly across (and individually in) each of the five fibroblast cell strains and the public data sets

In order to retrieve the genes most significantly differentially regulated with age across all the five fibroblast cell strains and the public data sets, we applied a stringent selection criteria of p<0.05 according to both statistical packages (DESeq and edge R) and minimum RPKM of 5

in either young or old samples for the five fibroblast cell strains and p<0.05 according to *limma* for the public data sets (adjusted p-values used).

Gene set enrichment analysis to determine the most differentially regulated pathways on aging

We used the R package *gage* [75] in order to find significantly enriched KEGG pathways. In case of our RNA-seq data the calculation was based on the gene counts and was performed as described in the methods manual. For the public microarray data sets, the calculation was based on log2 fold-changes estimated by *limma*. Estimated p-values were adjusted using the Benjamini and Hochberg's approach for controlling false discovery rate. KEGG pathways were selected as significantly regulated if the corrected p-values were smaller than 0.05.

Results

Growth curve of fibroblasts and transition into senescence

We selected five different fibroblast cell strains (MRC-5, BJ, IMR-90, WI-38 and HFF) and monitored their replicative behavior during passaging into senescence. The similarities in gene expression profiles of primary human fibroblast strains derived from embryonic lung and foreskin were revealed by us previously [76]. We extended our previous study [76] with data obtained from further three fibroblast strains (BJ, IMR-90 and WI-38) in this study in order to essentially extend the statistical basis for deducing common age-driven changes in the transcriptome. In our analysis, the cell strains were derived from a single vial and were maintained in culture as triplicates from an early population doubling (PD) time point until they achieved senescence at late PDs (Fig 1A). The growth curve (Fig 1B) reveals that the starting PD of each of the fibroblasts differs according to the prehistory of the cells before arriving in our laboratory. For MRC-5 fibroblasts, the start PD was 30 for fresh vials ordered from ATCC. For BJ, IMR-90 and WI-38 the start PD was between 20 and 30. HFF cells were freshly isolated from foreskin of young boys below the age of 10 at University of Erlangen. When the HFF strain samples were received for culture, the start PD was 14. The cell strain specific transition into senescence of each of the fibroblast cell strains was detected by the induction of SA-βGal with age. The assay was performed at intervals of every four PDs (Fig 1C). The induction of senescence was earliest in HFF and IMR-90 strains (Fig 1C) during their span in culture compared to the other three fibroblast cell strains while SA-β Gal increase was late for BJ fibroblasts. Indeed, BJ fibroblasts showed the most extended replicative lifespan (Fig 1B). IMR-90 and WI-38 fibroblasts, both derived from female lung, had the least cumulative PDs approaching replicative senescence much earlier than the other fibroblast cell strains (Fig 1B and 1C). Cell strain specific differences in growth and transition into senescence were reported and discussed by us before in a quantitative study [48]. Reassuringly, the growth curves of the fibroblast strains in our study are very similar to previously undertaken studies on fibroblast strains [48, 77, 78, 79]. In particular the growth curve we obtained for HFF is almost identical to the one obtained for HDFs in a previous study of gene expression profiles of replicative senescence [70].

For each of the five different fibroblast cell strains we defined three individual time points in each growth curve: young cells (early PD) at the beginning of the linear growth curve, old cells (late PD) at the final growth stage close to senescence, and middle aged cells (mid PD) half way between the two. Since WI-38 and IMR-90 cells reached senescence at considerably lower PDs (around 60 PDs) than MRC-5, HFF and BJ cells (between 72 and 76 PDs) (Fig 1B), the PD values for young, middle and old cells differ. For the five fibroblast cell strains, the transition into senescence measured by the percentage of SA-β Gal positive cells, analyzed at young, middle

and old stages of their lifespan, revealed a low standard deviation among the three parallel experiments of the triplicates (data not shown, see Materials and Methods), indicating that the observed differences in growth and transition into senescence are due to cell strain-specific properties and not due to experimental errors, consistent with our previous observations [48].

Correlation among the mRNA expression levels of fibroblast triplicates

Pellets of young, middle aged and old cells in triplicate were collected for the five fibroblast strains and total RNA was extracted. Among the mRNA expression levels measured by RNA-seq in the primary fibroblasts, correlations were deduced among the same fibroblast cell types depending on their age (i.e. mRNA data of low PDs were compared to those of high PDs) and among the five different fibroblast cell types.

The results revealed a significant correlation among the mRNA expression levels of the triplicates in all fibroblast cell strains. Sample clustering using multidimensional scaling (MDS) plots indicated that the expression of one late PD IMR-90 fibroblast sample (one of the three vials) showed increased variance (probably due to batch effects [80]) compared to the other two vials (S3 Fig); this outlying sample was removed from further analysis [81]. Taken together, our mRNA sequencing procedure resulted in a small technical error (mean Pearson's correlation of 0.98 within each group of replicates, one outlier removed). Clustering of the replicates in BJ and HFF (foreskin fibroblasts) was more obvious showing a larger correlation compared to IMR-90, MRC-5 and WI-38 (embryonic lung fibroblasts) (S3 Fig).

DEG in the five fibroblasts

The mRNA expression levels at young (low PDs) and old age (high PDs) were determined for each of the five fibroblast cell strains, and the DEG were deduced, i.e. for which mRNA expression levels significantly ($p < 0.001$) increased or decreased with age.

Validation of RNA sequencing results with real-time PCR

In order to validate our experimental approach, mRNA expression levels of selected genes in two fibroblast cell strains MRC-5 (human embryonic lung) and HFF (human foreskin fibroblasts) were analyzed using real-time PCR. We selected a set of genes which, in these two cell strains, were most differentially expressed with age (*CTSK*, *DKK3*, *TMEM47*, *CCNB1*, *CCNA2*, *C3*, *Wnt16*, *IGFBP2* and *CCND1*) and *p21*, expected to be significantly up-regulated with age [31, 82, 83]. We found that the results from real-time PCR correlated well in terms of the direction of regulation with the sequencing-derived mRNA expression levels (S4 Fig).

Comparison among the two hundred most differentially expressed genes in each of the five fibroblast cell strains

First, for each of the five fibroblast cell strains individually, we listed and analyzed the one-hundred most differentially up- (Fig 2, S5 Fig) and the one-hundred most differentially down-regulated (Fig 3, S6 Fig) genes with age.

When comparing these most differentially regulated genes between the two foreskin fibroblast cell strains (BJ and HFF), we identified 17 commonly up- (S2 Table) and 34 commonly down-regulated genes (S4 Table). The corresponding comparison between the three embryonic lung fibroblasts (MRC-5, IMR-90 and WI-38) revealed 10 commonly up- and 8 commonly down-regulated genes (S2 and S4 Tables). Then we compared the three lung fibroblast strains pairwise: MRC-5 and IMR-90 showed 25 commonly up- and 14 down-regulated genes, MRC-5 and WI-38 revealed 30 commonly up- and 16 down-regulated genes, while WI-38 and IMR-

MRC-5	HFF	IMR-90	WI-38	BJ
WNT16	TMEM176B	CCND2	CXCR7	CLDN1
CCND2	SYT1	TNFSF18	CD14	SLC38A11
TGFB2	CPXM2	ANKRD1	TMEM178B	COL8A1
PLCB4	CLSTN2	CPE	CCND2	AKR1B1
SLC14A1	TTC9	TGFB2	GDF6	PAPPA
CCDC68	TMEM178B	CDKN2B	TMEM176B	L1CAM
CTSK	PRELP	CTSK	FIBIN	TNFSF18
ADAMTS19	TACSTD2	CCDC68	CCDC68	CDH13
FILIP1L	TNXB	HIST1H2AC	ADAMTS19	IL1B
RGS4	INMT	PAPPA	PLAT	RP11-13L2.4
CADM1	IL17RB	MAMDC2	RP11-4F5.2	CTSK
RGS5	ENPP5	SHC2	GPC4	DRAM1
FIBIN	SLC38A11	SERPINE2	FGL2	RARRES2
TNFSF18	ENPP4	HIST1H4H	MCTP2	CLSTN2
A2M	SLC6A17	AMIGO2	SLC1A1	GM2A
UACA	PDGFD	MSMO1	LRRN4CL	IGFBP2
KCTD12	SH3BGRL2	CDKN2A	ADAMTS5	TNFRSF21
HIST1H2BK	PDE8B	TMEM159	CPE	F2RL2
ASAH1	PPP1R14A	MFAP4	ITGA8	IGFBP5
NEO1	ADAMTS5	EEF1A2	FUCA1	SYPL2
RGMB	PTGDS	IGFBP2	TXNIP	PRDX6
TMEM178B	CTSK	GFRA1	BMP2	HIST1H2AC
EDIL3	FMOD	VCAM1	KCNJ2	AGRN
MT2A	CHDH	ITGA11	C10orf10	EREG
ANKRD1	EPDR1	SLC5A3	SVEP1	ADAMTS5
HIST1H2AC	L1CAM	MT-CYB	DPP4	MKX
ACTA2	RAB11FIP2	FAM43A	TMEM47	FBLN1
LMOD1	CXCR7	MT-ND6	PRNP	TSPAN9
NIPAL3	LEPR	MT-ND2	FMOD	GNPTAB
CXCR7	TMTC1	NEO1	AKR1C2	CFH
PRSS23	GAS1	CYB5D2	PIK3IP1	PAM
ADAMTS5	PIK3IP1	PODN	SLC14A1	DUSP6
TMEM47	GRIA3	RRM2B	WNT16	C3
DYNLT3	HSPB7	ITGA11	PLEKHH2	CTSF
DKK3	RASSF2	CYBRD1	LACC1	SFRP4
MEGF9	AMIGO2	PTX3	TEK	RDH10
PBXIP1	QPRT	AKR1B1	RGS2	BTG2
INMT	TRPC6	NTM	C10orf54	CREG1
STC1	MFAP4	CADM1	HIST1H1C	PRAGMIN
PIK3IP1	FGF1	EPHX1	FILIP1L	C8orf4
PAM	IGFBP2	MT-ND5	A2M	SEMA3D
IGFBP7	SPON2	STEAP3	GBP2	C1QTNF1
WFDC1	FBN2	LUM	MEGF9	SOD2
SPON2	C13orf33	AKR1C1	CREG1	FUCA1
RRM2B	CCRL1	IGIP	MR1	HIST2H2BE
DCBLD2	TMEM47	TNFSF4	HEG1	SLC5A3
PROS1	CYBRD1	KCNE4	TMEM35	QPRT
EEF1A2	LTBP4	ITGBL1	ARRDC4	SRPX2
PCYOX1	CPQ	ADAMTS5		HIST1H2BK
WLS	ASAH1	MT-ND3		

Fig 2. Fifty most up-regulated genes with age in each of the five fibroblast strains. The red background represents genes commonly up-regulated with age in foreskin fibroblasts (HFF, BJ) and green background reveals genes commonly up-regulated among all the three embryonic lung fibroblasts (MRC-5, IMR-90, WI-38) as well as between the fibroblasts derived from female donors (IMR-90 and WI-38) among the hundred most differentially regulated genes with age.

doi:10.1371/journal.pone.0154531.g002

90, with 26 up- and 60 down-regulated genes, showed the highest number of commonly differentially regulated genes (S2 and S4 Tables). The observed differences among the three human embryonic lung fibroblasts (MRC-5, WI-38 and IMR-90) may reflect differences in the gender of the donor. MRC-5 was derived from male while IMR-90 and WI-38 were derived from female lung. Interestingly, the two female fibroblast strains IMR-90 and WI-38 both not only showed the highest number of commonly differentially regulated genes but also a considerably shorter lifespan compared to the other three fibroblast cell strains (Fig 1B and 1C).

If fibroblasts from the same tissue origin would behave similarly, we would expect a higher number of commonly differentially regulated genes amongst fibroblasts from the same tissue (foreskin or lung) than between fibroblasts from different tissues. In order to test this hypothesis, we determined the commonly regulated genes between each of the foreskin fibroblasts (HFF and BJ) on the one hand and each of the embryonic lung fibroblasts (MRC-5, IMR-90 and WI-38) on the other. HFF and MRC-5 showed 16 commonly up- and 15 commonly down-regulated genes whereas HFF and IMR-90 demonstrated 11 up- and 37 down-regulated genes while HFF and WI-38 revealed 14 up- and 41 down-regulated genes (S3 and S5 Tables). BJ and MRC-5 showed 13 up- and 11 down-regulated genes while BJ and IMR-90 revealed 18 up- and 42 down-regulated genes. WI-38 and BJ showed a different set of 18 commonly up-regulated and 52 commonly down-regulated genes (S3 and S5 Tables). These numbers do not systematically differ from the number of 17 commonly up- and 34 commonly down-regulated

MRC-5	HFF	IMR-90	WI-38	BJ
CYP1B1	FAM64A	PTTG1	POSTN	HAPLN1
ID3	MKI67	KIF20A	CDC20	TGFBI
PSAT1	MYBL2	CCNB1	ASPM	FBN2
HSPA5	CDC20	DLGAP5	MKI67	FST
CLDN11	DLGAP5	IQGAP3	LMNB1	EDIL3
HERPUD1	BEX1	PRC1	KIF4A	GLIPR1
COL15A1	KIFC1	LMNB1	KIF20A	IGFBP3
LRRN4CL	SCARA3	CCNB2	CENPF	LBH
CYBA	IQGAP3	NDC80	ANLN	HAS2
MTHFD2	ANLN	CENPF	DLGAP5	ELN
SERPINH1	ID1	ID3	UBE2C	PPAP2B
ID1	TK1	MAD2L1	KIF14	SEMA7A
NID2	RRM2	UBE2C	RRM2	ACTA2
ICAM1	SHCBP1	GGH	NCAPG	FN1
SDC1	CEP55	CENPW	CEP55	BGN
NFKBIZ	TOP2A	CDC20	BIRC5	MFAP5
FAM129A	TBX4	CCNA2	SHCBP1	EGR1
SLC3A2	WNK4	KIF14	TOP2A	SCARA3
PEAR1	CXCL12	TK1	PLK1	FGF5
SCD	PTTG1	KIF11	TK1	CDC42EP3
MANF	SPAG5	TNFRSF19	CDK1	CENPF
HYOU1	TPX2	RNASEH2A	PRC1	PTGIS
PHGDH	NR4A1	TOP2A	KIF11	LTBP1
IL8	PRC1	PBK	CCNA2	TMPO
OLFML3	RPL22L1	TMSB15A	BGN	CRLF1
CRABP2	CCNB1	SPAG5	TPX2	ANKRD1
DDIT3	BGN	BIRC5	IQGAP3	FAM180A
NDN	SPHK1	PRRX1	ARHGAP11A	CXCL12
SLC1A5	ENPP2	SGOL2	COL4A1	CEP55
PCOLCE	TBX2	SHCBP1	FOXM1	ITGBL1
LOXL3	RGS4	ARHGAP11A	FAM64A	KIAA1462
MYC	F3	SPC24	CDCA8	C4orf3
COL5A3	CA12	PCOLCE	SPAG5	METRNL
POSTN	TYMS	TACC3	AURKB	RGS4
INSIG1	TGM2	DHFR	PTTG1	EFEMP1
TNFRSF19	CCNB2	SDC1	CCNB1	CTHRC1
LOXL4	MYC	GPC6	KIFC1	ANLN
SLC39A14	ID3	TYMS	PBK	ASPM
SDF2L1	STMN1	RFC3	CCNB2	HSPB6
SLC7A5	COTL1	NCAPG	COL4A2	STMN1
SLFN11	KIF11	CKS2	CTHRC1	BIRC5
TMEM119	TRIB1	IL11	CLDN11	POSTN
MDK	ZWINT	TPX2	HJURP	GREM2
FADS2	FAM167A	SOCS1	ZWINT	OLFML3
PTMA	HMGN2	ANLN	FAM83D	TOP2A
PDIA4	PTGS1	CDCA8	G0S2	KIF20A
TRIB3	KIF20A	AURKB	TRIP13	FOXM1
CRELD2	C1orf115	MCM6	TACC3	KLF6
DUSP5	AURKB	GINS2	CDCA5	CYP1B1
PRRX1	HMGA1	UBE2S	MLF1IP	HMGB2

Fig 3. Fifty most down-regulated genes with age in each of the five fibroblast strains. The red background represents genes commonly down-regulated with age in foreskin fibroblasts (HFF, BJ) and green background reveals genes commonly down-regulated among all the three embryonic lung fibroblasts (MRC-5, IMR-90, WI-38) as well as between the fibroblasts derived from female donors (IMR-90 and WI-38) among the hundred most differentially regulated genes with age.

genes between HFF and BJ fibroblasts (see above). This indicates that the observed differences with age among the commonly differentially regulated genes across the five fibroblasts do not seem to originate from the different cell sources.

Taken together, among the five analyzed fibroblast cell strains, we found common transcriptional regulation (a mean of 19% commonly up- and 32% commonly down-regulated genes) but also considerable cell strain specific differences in the set of genes most differentially expressed after transition into senescence.

Comparison of our study in the five fibroblast strains with previously published studies on primary human fibroblast strains

We then compared our results with similar published data [28, 64–71]. None of these published data relied on RNA-seq as in our study. The highest number of commonly regulated genes was found when we compared our mRNA expression data for each of the fibroblast cell

strains individually with those retrieved from HFF strains by [67]. Several of the up-regulated genes belong to the family of insulin like growth factor binding proteins. *IGFBP3*, a marker for cellular senescence [84], is up-regulated across HFF strains in our study as well as in the study conducted by [67] and in IMR-90 fibroblasts [69]. *IGFBP5*, induced during cellular senescence [85], is up-regulated across BJ fibroblasts in our study, dermal fibroblasts [65] and in HFF strains [67]. *IGFBP2*, significantly up-regulated with senescence in retinal pigment epithelial cells [86, 87], is up-regulated in both foreskin fibroblasts (HFF and BJ) in our study and in human dermal fibroblasts [70]. *HAS2*, involved in wound healing and tissue repair [88], is down-regulated in both IMR-90 in our study and in HFF strains [67]. The most differentially regulated genes with age *KIF20A*, *KIF11*, *CCNB1*, *CCNB2*, *ANLN* and *TOP2A*, identified by [67] were also among the most commonly differentially regulated genes among the five fibroblasts in our investigation. We found a high degree of similarity between common DEG among MRC-5 fibroblasts in our study and that conducted by [68], HFF strains conducted by [67] and human dermal fibroblasts conducted by [70]. A similar high number of common DEG was retrieved on separately comparing IMR-90 and WI-38 fibroblasts in our study with the HFF data of [67] and the IMR-90 data of [71]. Thus, our RNA-seq derived transcriptome signatures of replicative senescence are fully consistent with previously published data based on gene arrays.

Next we determined the common most significantly differentially regulated genes across the five fibroblast cell strains and a sub-selection of five published data sets [64, 65, 67, 68, 70]. The stringency criteria of $p<0.05$ according to statistical packages (DESeq and edge R), a minimum RPKM of 5 in either young or old cells for the five fibroblast cell strains, and $p<0.05$ according to *limma* / adj.pvalue for the public data sets were applied. This comparison resulted in 15 up- and 7 down-regulated genes. All these genes have been annotated to specific pathways (as described in http://www.genecards.org and http://www.reactome.org). The up-regulated genes included those associated with metabolism (*RRM2B*, *HEXB*, *AKR1B1*, *SMPD1*, *PEA15*), cell cycle (*CCND1*, *DYNLT3*), apoptosis (*MOAP1*, *SERINC3*) or with membrane transport and signaling, i.e SASP (*NPC2*, *ZMAT3*, *TNFRSF10D*, *LRP10*). The down-regulated genes were associated with cell cycle (*MCM6*, *CDC6*, *SET*, *RAD21*), cellular functions (*AXL*) or mRNA splicing (*HNRNPM*, *SNRPD1*).

Common DEG with age across the five fibroblast strains

In order to identify specific senescence-associated genes, we extracted those that were most significantly commonly differentially expressed with age across all of the five fibroblast cell strains. While the most differentially expressed genes were listed and compared for every one of the five cell strains independently (as mentioned in section entitled "Comparison among the two hundred most differentially expressed genes in each of the five fibroblast cell strains"), now those genes were deduced which were most differentially expressed commonly amongst all five cell strains together, applying the selection limit $p<0.05$. Of the 24,357 annotated genes, 2088 protein coding genes were affected by age among the five cell strains (8.6%). From these genes, 705 were commonly up- and 915 commonly down-regulated in all five strains while 468 genes were inconsistently regulated. Thus, 78% of the age affected DEG were commonly regulated in the same direction (either up- or down-regulated) in all five fibroblast strains. This high number indicates a strong conservation of replicative senescence associated changes in the transcriptome with only a minor strain-specific contribution, consistent with our earlier findings [76].

We then implemented more stringent selection criteria: $p<0.001$, log2 fold change >1, and adherence with both statistical packages (DESeq and edgeR). This very stringent selection still

resulted in over 500 identified genes. When increasing the stringency of selection even further (now requiring an additional stipulation of (i) mean RPKM value >5 in each of the five fibroblast cell strains and (ii) a combined mean RPKM value >5 among the five fibroblast cell strains), 18 commonly differentially regulated genes were identified among the five different fibroblast cell strains: 2 up-regulated genes (*HIST1H1C* and *RRM2B*) and 16 down-regulated genes (*ANLN, UBE2T, TPX2, KIF20A, RNASEH2A, CDC20, TOP2A, KIF11, CCNB1, CEP55, CCNB2, TK1, HMGB2, RRM2, CENPW* and *KIFC1*). A number of these genes, including *RRM2B, ANLN, KIF20A, TOP2A, KIF11, CCNB1* and *CCNB2*, have already been identified by analyzing the five fibroblast cells strains independently with previously published studies (section entitled "Comparison of our study in the five fibroblast strains with previously published studies on primary human fibroblast strains"). Thus, even under strongest selection criteria, a set of genes commonly associated with the aging process in all five fibroblast strains can clearly be identified, irrespective of analyzing the cell strains independently or commonly. These genes were further investigated. For these 18 genes in each of the five fibroblasts, the protein expression levels were determined quantitatively by immunoblot band intensities. For all these 18 genes, up- or down-regulation of mRNA and protein expression values correlated well during aging (Data not shown). Thus, among the five fibroblast cell strains we could identify, even under highest selection criteria, a number of genes commonly associated with the transition into senescence. These genes of the five strain comparison overlap to some extent but not completely with those genes found by us for a two strain comparison [76]. This emphasizes the importance of increasing the number of cell strains for deducing common age-driven transcriptome changes in the cell strains. Nevertheless, the overall conclusions remain unchanged.

However, surprisingly senescence associated cell cycle inhibitors p16 (*CDKN2A*), p15 (*CDKN2B*), p21 (*CDKN1A*) and p27 (*CDKN1B*) were not among the significantly differentially regulated genes with age among the fibroblast strains. These genes are usually found to be significantly up-regulated with age in fibroblast cell strains [18]. We therefore determined, in immunoblots, the protein level of these four genes for the triplicates of the five fibroblast cell strains maintained in culture from low to high PDs. The results revealed significantly higher protein levels of p16, p15, p21 and p27 with age in all five fibroblast cell strains confirming earlier findings on the role of p16 [24, 44], p21 [21, 23, 43], p27 [18, 89–91] and p15 [18, 92] in senescence induction. We found that mRNA and protein levels correlated only in some of the fibroblast strains. This selective lack of correlation of mRNA and protein expression levels has been observed before [70, 93, 94]. However, the strong up-regulation of p16 during replicative senescence in BJ fibroblasts observed here, does not agree with previous studies [95, 96]. Thus, depending on cell strain, the age-dependent protein expression of p15, p16, p21 and p27 is regulated at the transcriptional level in some but by other down-stream mechanisms in other cases.

Commonly regulated pathways with age

Commonly regulated pathways among the five fibroblast strains.   Next, we identified the pathways most differentially up- or down-regulated with age by performing gene set enrichment analysis using the R package *GAGE* (Generally Applicable Gene-set Enrichment) in combination with all annotated KEGG pathways separately for each of the five fibroblast cell strains. The most differentially up- and down-regulated pathways in each of the five fibroblast strains are listed in S6 Table. Then, we combined all found pathways and filtered them according the same direction of regulation in all five cell strains, resulting in 36 up- and 32 down-regulated pathways (Fig 4). When applying p<0.05 as selection criteria, we found 13 pathways to be commonly down-regulated in all five cell strains, among them the well-known senescence-

associated ones, such as "DNA replication (hsa03030)", "Cell cycle (hsa04110)", and DNA repair pathways ([Fig 4](#)), consistent with [97]. As potentially novel common down-regulated pathways we found "Spliceosome (hsa03040)", "RNA transport (hsa03013)", "Ribosome biogenesis (hsa03008)", and "Pyrimidine metabolism (hsa00240)" ([Fig 4](#)). The "Spliceosome (hsa03040)" pathway is also down-regulated with age in brains of *N. furzeri* [98].

Common pathways across the five fibroblast strains and previously published datasets. Next, we compared our RNA-seq data with eight studies which, by using microarray measurements, had investigated transcriptomic changes during replicative senescence in human fibroblasts. Here, the pathways identified by us were related to pathways based on these
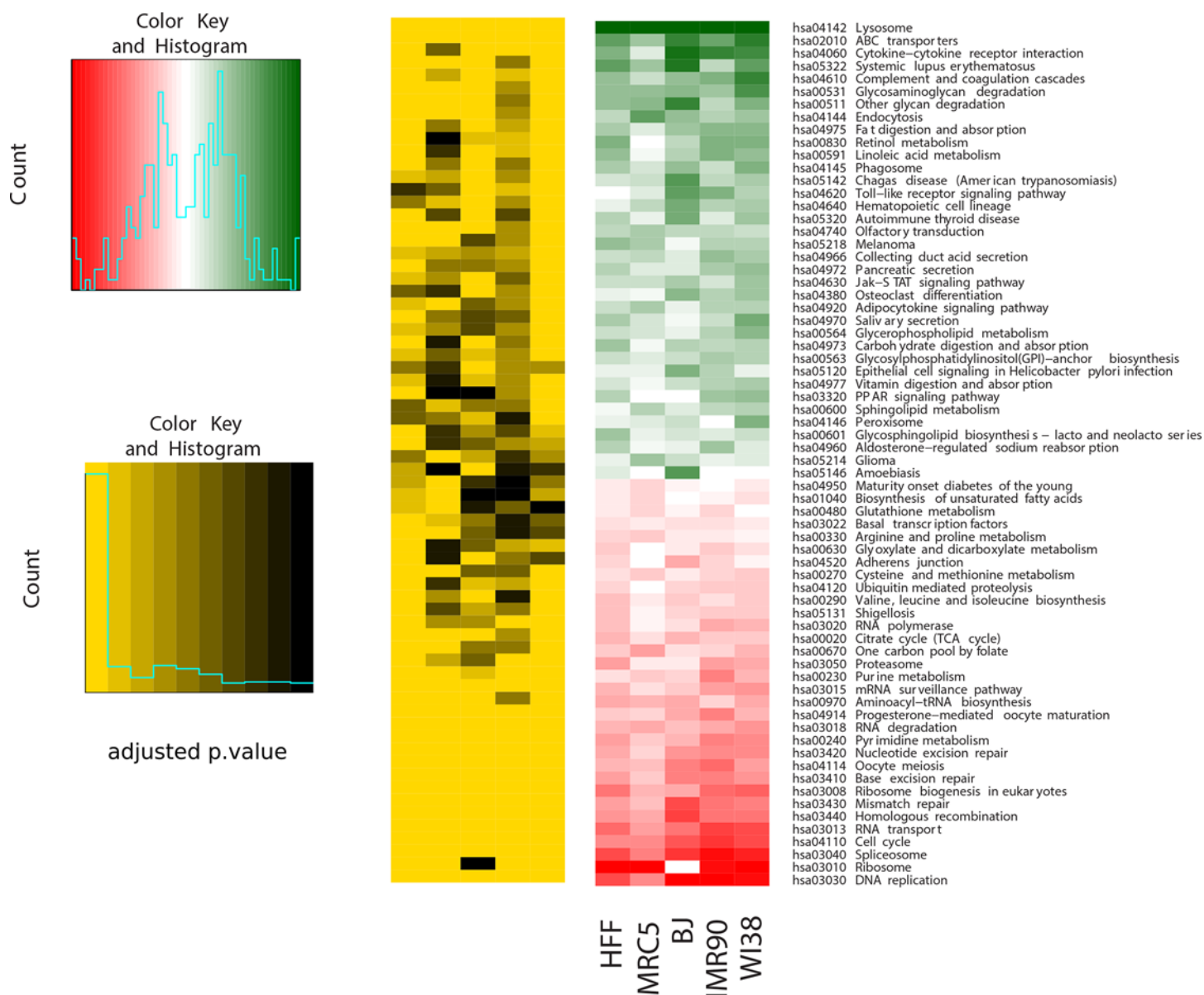
Fig 4. Significantly differentially regulated pathways with age across the five fibroblast strains. The most significantly up- and down-regulated pathways across the five fibroblast strains retrieved by performing gene set enrichment analysis by applying the R package *gage* (Generally Applicable Gene-set Enrichment) in combination with all annotated KEGG pathways separately for each of the five fibroblast strains.
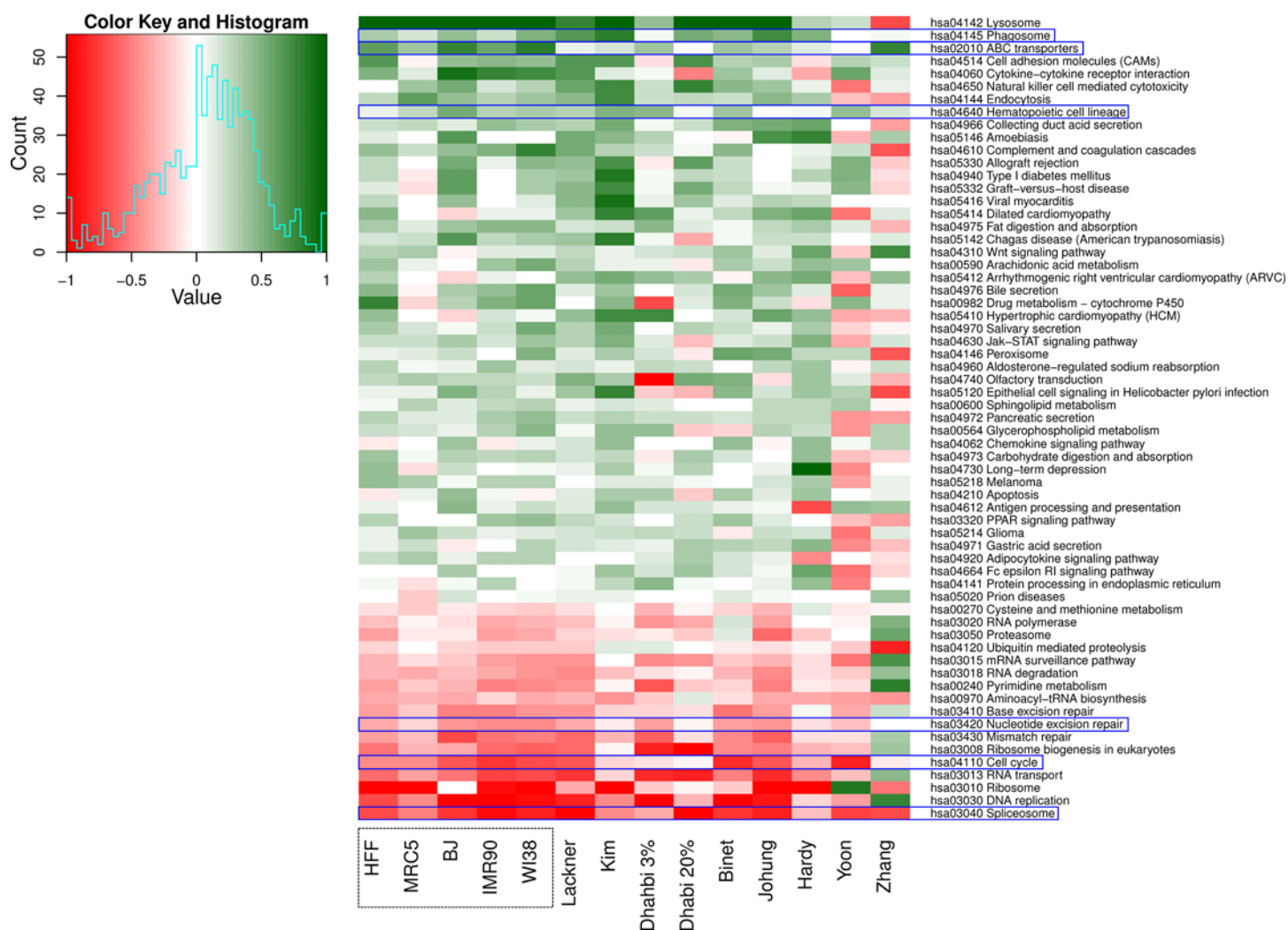
doi:10.1371/journal.pone.0154531.g004

Fig 5. The differentially regulated pathways across the five fibroblast strains and the public data sets. The most significantly up- and down-regulated pathways across the five fibroblast strains and the nine selected public data sets retrieved by performing gene set enrichment analysis. Pathways highlighted with blue rectangles have similar regulation pattern across all the 14 datasets.

doi:10.1371/journal.pone.0154531.g005

eight studies. Since pathways group a number of genes, first we treated the transcriptome data as described below.

The raw data were downloaded either from GEO at NCBI or from ArrayExpress at EBI. We repeated our data analysis for the published data in order to obtain fold-changes for all measured genes available on the respective microarrays, and subsequently identified DEG using the R package *limma*. Fig 5 includes 14 different data sets: five different datasets, one for each cell strain, from this study and nine published data sets (two data sets derived from one study by [69]). Not every gene could be compared across all 14 data sets due to either missing probes on the microarray or differences within available annotation and gene ID conversion. For all comparable genes, we created pairwise scatterplots of the fold-changes, estimated their correlation and determined the number of commonly regulated genes (either up- or down-regulated with

increasing PD; data not shown). For 76 out of 91 possible pairwise comparisons, more than 50% of all 1,334 comparable genes exhibited the same direction of regulation (mean = 58 ± 7%). For 79 out of the 91 comparisons, the comparable genes showed positive correlation of log2 fold-changes (mean 0.19). These results indicate both, similar regulation patterns within our data and a considerable fraction of genes with similar expression through different studies and cell strains.

We then applied gene set enrichment analysis for the nine published data sets analogous to the approach used for our five data sets. We filtered the resulting pathways for common direction of regulation for 11 out of all 14 data sets, which resulted in 46 up- and 17 down-regulated pathways (Fig 5). Notably, "Nucleotide excision repair (hsa03420)", "Cell cycle (hsa04110)" and "Spliceosome (hsa03040)" were found again to be down-regulated in all the data sets (in Fig 5 marked with blue rectangles). As among the five fibroblast cell strains studied here, "Lysosome (hsa04142)" was one of the significantly up-regulated pathways with age among the four published data sets [67, 68, 70, 71]. From the remaining four published data sets [64–66, 68]; no significantly up-regulated pathways were obtained. The three pathways "Phagosome (hsa04145)", "ABC transporters (hsa02010)" and "Hematopoietic cell lineage (hsa04640)" exhibit similar regulation patterns in all the data sets investigated in this study. Interestingly, the up-regulation of these three pathways with age has not been explicitly shown previously in none of the human fibroblast strains investigated in this study. However, up-regulation of expression of a number of genes associated with the regulation of the "Phagosome (hsa04145)" and "ABC transporter (hsa02010)" pathway with age was described for other cell systems [99, 100]. Furthermore, ABC transporters have been associated with providing resistance against multiple drugs in a number of cancers [101]. The up-regulation in hematopoietic cell lineage pathway with increased age was unexpected since the renewal capability of hematopoietic stem cells, originating from the hematopoietic cell lineage, decreases with age [102]. We found the same set of pathways significantly up- or down-regulated when studying two fibroblast strains (MRC-5 and HFF) [76].

Further, we undertook an in depth comparison of expression data from our five cell strains with IMR-90 microarray data from a similar study [71]. 15,278 genes were available on the microarray and included in the annotation of our RNA-seq data. IMR-90 cells from both studies behaved in a similar fashion with 74% of the genes commonly up- or down-regulated (Pearson's correlation was 0.49 for log2 fold-changes between early and late PDs). IMR-90 cells by [71] behaved also very similar to our WI-38 cells (78% of genes with same direction of regulation; Pearson's correlation of 0.54 for log2 fold-changes).

Functional validation of selected genes most differentially expressed with age

Next, we investigated the expression levels of genes associated with SASP, containing proteins that were up-regulated with induction of senescence [103, 104]. As expected, a number of genes associated with SASP were significantly up-regulated with age in MRC-5 and HFF strains. The list of genes also included *IGFBP7* and *MMPs* (S4A and S4C Fig) which have been previously found to be up-regulated with senescence in other cell types [30, 104–106].

In addition we found *SFRP4* and *DKK3*, both contributing to Wnt signaling [107, 108], significantly up-regulated with age in foreskin fibroblasts in terms of both mRNA and protein expression levels (HFF and BJ). *DKK3*, but not *SFRP4*, was also significantly up-regulated with age (both mRNA and protein levels) in embryonic lung fibroblasts (MRC-5, IMR-90, and WI-38). In order to determine whether *SFRP4* and *DKK3* have an impact on fibroblast senescence, we added recombinant SFRP4 protein to culture media of foreskin fibroblasts (HFF and BJ).

We verified cellular protein up-take from the media by measuring SFRP4 protein levels in fibroblasts maintained in media containing recombinant SFRP4 proteins. Cellular protein intake was indicated by the protein bands in immunoblots for HFF, BJ and MRC-5 cells. Treatment of HFF strains (PD = 18) with 15 µg/ml human recombinant SFRP4 protein for 10 days revealed an up-regulation of SA-β Gal in some but not all cells (26–28% of the cells, Fig 6A).
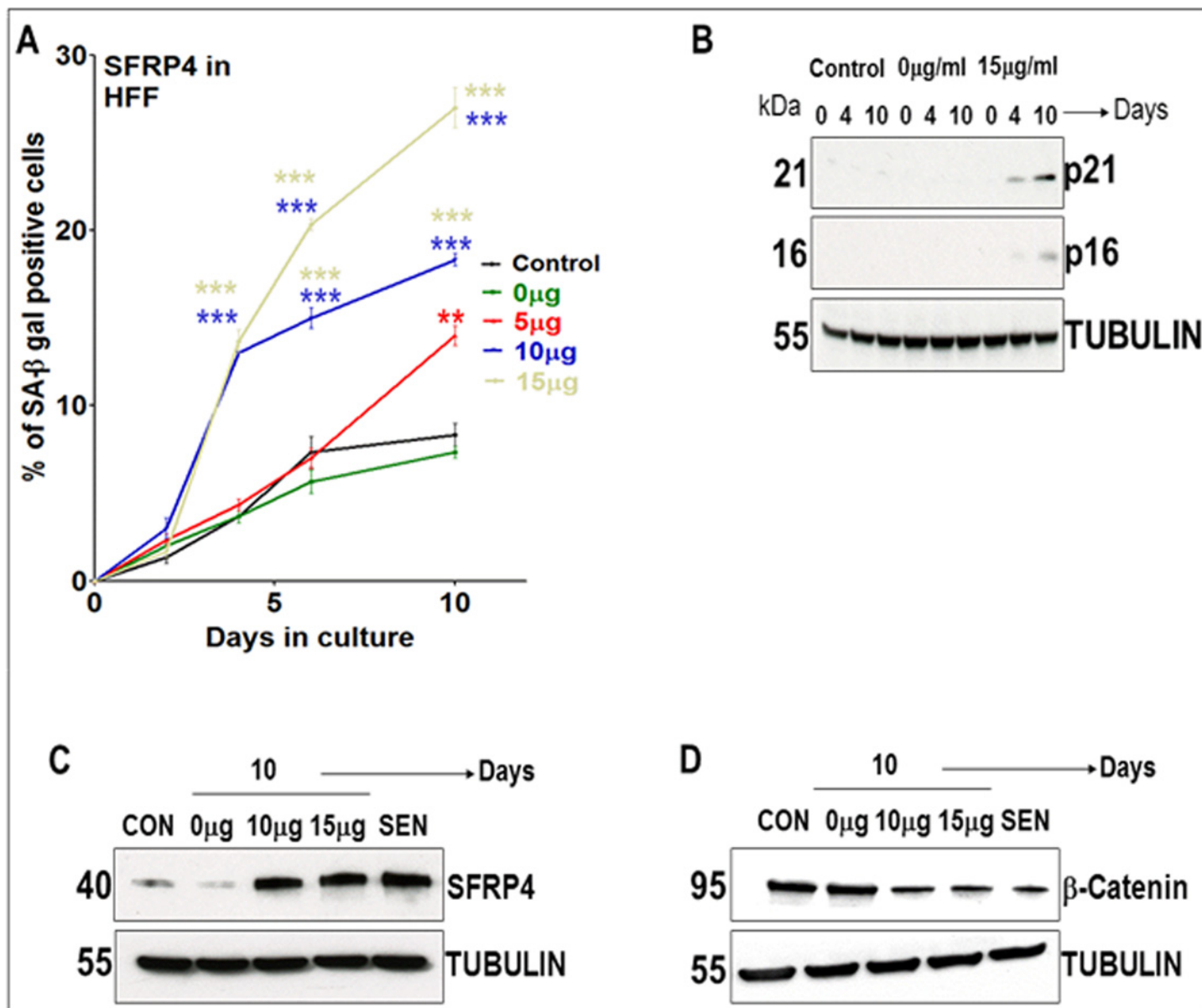

Fig 6. Recombinant human SFRP4 protein treatment in human foreskin fibroblasts (HFF). (A) Percentage of SA-β Gal positive cells at different time points up until 10 days in HFF strains (PD = 18) maintained in conditioned medium containing different concentrations of recombinant human SFRP4 (rSFRP4) proteins (0, 5, 10, 15 µg/ml). Samples specified control were untreated fibroblasts and those specified treated with 0 µg were treated with PBS containing 0.1% Bovine serum albumin instead of rSFRP4. The bars indicate the mean ± S.D. Values statistically different from their controls (Student's t-test, 95% confidence level) are indicated with an asterix. ** p < 0.01, *** p <0.001- Significantly different compared to controls. n = 3 (B) Results of quantitative immunoblots showing protein expression levels of p16 and p21 in HFF strains treated with 15 µg/ml recombinant human SFRP4 proteins compared to controls and HFF strains treated with 0 µg SFRP4. n = 3 (C) Immunoblot shows protein expression levels of SFRP4 in control (CON; PD = 18), senescent (SEN; PD = 74) and young fibroblasts (PD = 18) maintained in culture supplemented with conditioned medium containing 0, 10 or 15 (µg/ml) rSFRP4 proteins for 10 days. n = 3 (D) Immunoblot shows protein expression levels of β-Catenin in control (CON; PD = 18), senescent (SEN; PD = 74) and young fibroblasts (PD = 18) maintained in culture supplemented with conditioned medium containing 0, 10 or 15 (µg/ml) rSFRP4 proteins for 10 days. n = 2.

doi:10.1371/journal.pone.0154531.g006

p16 and p21 protein expression levels increased due to recombinant protein treatment (Fig 6B), supporting initiation of senescence induction. In order to investigate the possible antagonistic impact of SFRP4 treatment on Wnt signaling, we investigated the accumulation of β-Catenin which is functionally linked to SFRP4 [109]. β-Catenin nuclear accumulation facilitates tumor progression. β-Catenin mRNA and protein expression levels in control HFF strains decreased with age. Recombinant SFRP4 treatment down-regulated β-Catenin levels (Fig 6D), consistent with published observations [110]. With increasing amounts of recombinant human SFRP4 protein, SA-β Gal was induced (Fig 6A). Increasing SFRP4 levels in the media of young PD HFF strains further to 25 and 30 μg/ml did not induce higher SA-β Gal levels but still decreased β-Catenin levels. We obtained similar data for SFRP4 treatment in young BJ fibroblast strains (PD = 34) with 10 or 15 μg/ml. Thus, by preventing β-Catenin accumulation in HFF and BJ strains, human recombinant SFRP4 treatment (15, 25 and 30 μg/ml) may block cell proliferation. In contrast to these results obtained for HFF and BJ, adding up to 15 μg/ml recombinant SFRP4 to the culture media of embryonic lung fibroblasts (MRC-5) did neither induce SA-β Gal nor decrease β-Catenin levels. Thus, MRC-5 cells are non-responsive towards SFRP4 senescence induction signaling compared to HFF and BJ strains.

Three months after the induction of senescence (>90% SA-β Gal positive cells) in HFF and BJ fibroblast cultures, no significant changes in SFRP4 levels were observed. Since SFRP4 protein is able to initiate an induction of pre-mature senescence in young PD HFF strains (revealed by 26–28% of β Gal positive cells, Fig 6), we now asked if siRNA knock-down of SFRP4 in old (PD = 60) HFF strains (>60% SA-β Gal positive cells) can reduce the level of senescence as indicated by the number of SA-β Gal positive cells. First we verified that SFRP4 knock-down was successful. Using various concentrations ranging from 0 to 150 nM, we did not observe any effect of SFRP4 knock-down on the number of SA-β Gal positive HFF cells and on β-Catenin protein expression levels.

Then, we studied the influence of DKK3 ("dickkopf") levels on senescence. We asked whether exogenous administration of DKK3 may initiate signaling leading to senescence induction. We thus supplemented young HFF (PD = 22) strains with recombinant DKK3 proteins (0–50 μg/ml). However, there was no effect on senescence induction. HFF strains were chosen for recombinant DKK3 protein treatment because these fibroblasts were the most sensitive to recombinant SFRP4 treatment. These experiments suggest that SFRP4 and DKK3 have no well-defined common impact on senescence induction in the fibroblast strains studied here.

Discussion

Here we established by RNA-seq the transcriptome signature of replicative fibroblast senescence at unprecedented high resolution. Our data sets are expected to be more comprehensive as the previously published studies were based on microarrays. RNA-Seq is superior in detecting low abundance transcripts, differentiating biologically critical isoforms, a broader dynamic range, and detection of more differentially expressed genes with higher fold-change. Another benefit of RNA-seq is avoidance of technical issues inherent to microarray probe performance such as cross-hybridization, non-specific hybridization and limited detection range of individual probes [111].

By comparing the RNA-seq profiles obtained for five different fibroblast strains (MRC-5, HFF, WI-38, IMR-90 and BJ) we were able to delineate fibroblast strain-specific signatures as well as the pathways common to all of them. These data are expected to serve as an important information repository for future research on cellular aging.

Genes most differentially regulated with age individually in each of the five fibroblast cell strains

We determined the genes most differentially regulated with age individually in each of the five fibroblast cell strains. The two female lung fibroblasts showed more similarities amongst them than compared to the other three cell strains; nevertheless, the observed differences in DEG were not significantly larger between the lung and foreskin fibroblasts than between cell strains from the same source. Thus, the observed differences were not mainly due to the different cell origin. Among the five analyzed fibroblast cell strains, we found cell strain specific differences in the senescence-associated genes, however, amongst subsets of these cell strains we identified a number of genes commonly regulated during the transition into senescence.

Most previous studies on age related changes in gene expression in human fibroblasts analyzed replicative aging only in single fibroblast cell strains [28, 65–71], only [64] studied expression values in the three fibroblasts WS1, WI-38 and BJ. Comparing data of each of our five fibroblast cell strains with these published results revealed not only a considerable similarity between our data and several published expression profiles, in particular with [67], [68], [70], [71], but also revealed several new aspects.

Genes commonly regulated among all five fibroblast strains

Across the five fibroblast cell strains, we determined the most significantly commonly differentially expressed genes with age. From the total of 24,357 annotated genes, 78% of the age affected DEG was commonly regulated in the same direction (either up- or down-regulated). We thus found a strong conservation of age-associated changes in the transcriptome with a 22% strain-specific contribution. Interestingly, we had found the transition into quiescence [35, 112] and the hormetic response to rotenone addition [113] strongly influenced by cell strain specific effects.

By applying very stringent statistical selection criteria, we revealed those genes which were most differentially regulated commonly with age among all of the five fibroblast cell strains. A number of these genes were also identified by analyzing the five fibroblast cell strains independently. The protein expression levels of these 18 genes correlated well with the mRNA expression levels of each of these genes, indicating that the expression of these proteins is regulated at the transcriptional level. However, in some cell strains, the protein expression of some CDK inhibitors was found not to be regulated solely at the transcriptional level (see section "Common DEG with age across the five fibroblast strains"). The functional annotation of these genes with software DAVID [114] revealed that most of the 18 commonly differentially regulated genes with age were cell cycle regulatory genes. Previous studies in various cell types demonstrated an association of almost all of the above genes with proliferation, cell cycle arrest or senescence [28, 115–135].

Together with the above genes, it was also interesting to note a significant down-regulation of FOXM1 mRNA expression levels across all the five fibroblast cell strains. FOXM1 is a major transcription factor having a role in cell cycle progression, mitotic division, genomic stability as well as expression of a number of G2/M phase specific genes including CENPF and CCNB2 [136, 137]. Also the mRNA expression of the transcription factor E2F1 is significantly down-regulated with age across all five fibroblast cell strains, but to a lower extent when compared to the down-regulation of FOXM1. E2F1 induces a senescent phenotype when over-expressed in normal human fibroblasts [138]. Furthermore, extracellular matrix-remodeling genes (MMP-1, Stromelysin-1^{MMP-3}, and PAI-1^{SERPINE1}) are also up-regulated in senescent WI-38 fibroblasts [138]. MMP-1 was significantly up-regulated with age only in HFF and WI-38 fibroblasts whereas Stromelysin-1^{MMP-3} was significantly up-regulated with age in HFF and PAI-1^{SERPINE1}
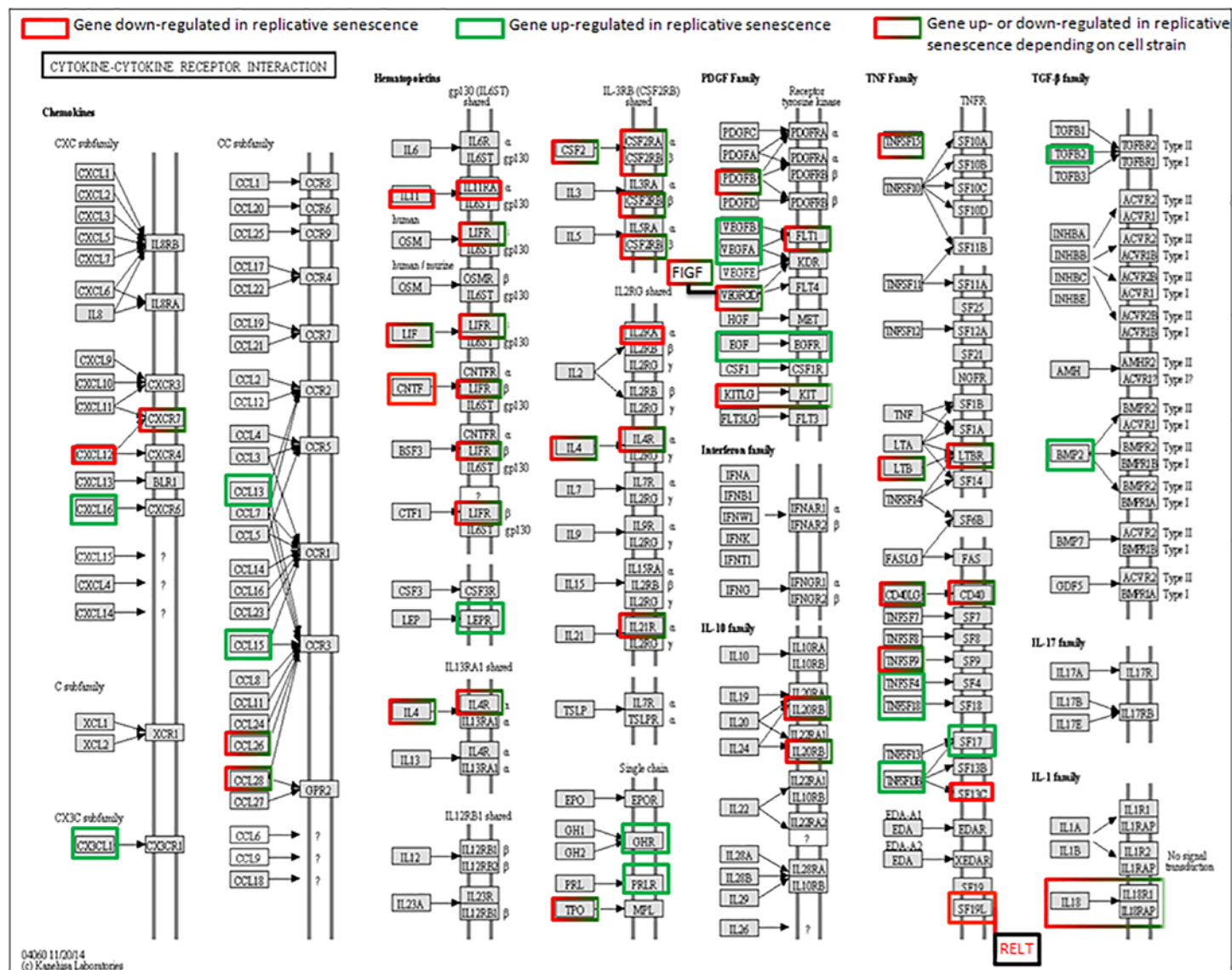
in MRC-5 fibroblasts, indicating cell strain specific differences. Though we found other transcription factors including ATF1 [139, 140], HSF1 [141, 142], CREB1 [143] and NFκB1 [144] down-regulated with age among at least three of the five fibroblast cell strains, they were not down-regulated to a significant extent. Additional experiments are required in order to understand the mechanism(s) responsible for their down-regulation.

Pathways commonly differentially regulated among the five fibroblast cell strains

We also elucidated the KEGG pathways most differentially regulated with age among the five fibroblast cell strains. Gene set enrichment analysis resulted in 36 up- and 32 significantly down-regulated pathways (Fig 4). DNA repair and cell cycle associated pathways were most prominently represented among the down-regulated pathways (Fig 4). Down-regulation of pathways associated with cell cycle progression was expected for the age-related induction of senescence. Previously we observed that the high levels of DNA damage found in old cells, were not repaired [35], explaining the oxidative DNA damage increase with age. This age-related DNA damage increase is explained properly by the down-regulation of DNA repair pathways with age [35], as found here. Among the commonly regulated pathways were some with most and some with only very few genes regulated but also mixed pathways (either with some genes up- and some down-regulated, or with some genes up-regulated in some strains but down-regulated in others). Currently we are studying in detail the genes belonging to these pathways and for future functional studies, the role of the age-dependent differentially regulated genes in pathway function will be considered. However, elucidating the mechanism responsible for the down-regulation of DNA repair and cell cycle associated pathways, and whether the down-regulation is a cause or consequence of senescence, needs further experimentation.

Senescence associated secretory phenotype (SASP)

As expected, several genes associated with SASP were found to be most differentially regulated with age in the five fibroblast cell strains. SASP is an important hallmark and functional mediator of senescent cells [31]. In order to assess SASP expression at the transcriptional level, we visualized within the KEGG pathway "cytokin-cytokine receptor interaction" (hsa04060) the genes differentially regulated in all five fibroblast strains (Fig 7). This pathway is significantly up-regulated across all the five fibroblast strains. While, as expected, strong up-regulation was found for many cytokines and cytokine receptors (i.e. TGFB2, BMP2, CXCL16, EGF, EGFR) in all cell strains (Fig 7, marked green), the mRNA levels of many other factors within this pathway were not found to be up-regulated, or even were down-regulated (i.e. CXCL12, IL11) (Fig 7, marked green). In addition, several of the signaling factors were up- or down-regulated cell strain specifically (IL4, IL4R) (Fig 7, marked green and red). We conclude from these observations that at the transcript level SASP regulation is very heterogenous. SASP assessment may be more reliable by directly measuring protein levels. This is consistent with a detailed SASP study showing that antibody arrays provide a much more accurate assessment of the SASP signature than mRNA profiling [83]. Nevertheless, the global up-regulation of the "cytokin-cytokine receptor interaction" pathway in all fibroblast strains (Fig 7) along with the strong up-regulation of related pathways ("Cell adhesion molecules"; ABC transporters; "Endocytosis"; "Complement and coagulation cascades") in individual strains (S6 Table)) fully confirm a strong induction of the secretory phenotype in all fibroblast strains analyzed here.

Fig 7. Genes belonging to the cytokine-cytokine receptor interaction pathway which are significantly up- (green) or down- (red) regulated (log 2 fold change > 1) across the five fibroblast strains during replicative senescence. Genes highlighted with boxes colored red+green are up-regulated in certain and down-regulated in the other fibroblast strains.

Conclusion

We conducted a comprehensive replicative aging study in five human fibroblast strains in parallel and extensively compared ours with previously published results. The complete age-dependent gene profiles were determined by RNA-seq in triplicates. This is an unbiased approach, unlike array analyses, as transcription of all genes was determined quantitatively and redundantly. We identified a high number of commonly up- and down-regulated genes as well as pathways, irrespective of analyzing the human fibroblast strains independently or commonly. For some proteins, changes with age in protein levels were not related to the corresponding changes of mRNA levels, indicating a down-stream protein expression regulation. First functional studies, conducted by us based on our data, confirmed the involvement of the secretory pathway in aging. Currently we are investigating the regulation of genes belonging to the commonly differentially

regulated pathways across the five fibroblast strains as well as the proteome profile of aging primary human fibroblasts. These studies together with the transcriptome data presented here will enable an even deeper insight into the cellular aging process.

Data deposition

All reads have been deposited in the NCBI GEO under the accession number GSE63577 and will be made available at the time of publication.

Ethics Statement

The human fibroblast cell strains (MRC-5, IMR-90, WI-38 and BJ) used in this investigation was ordered from ATCC. A number of senescence related studies has been undertaken using these fibroblast cell strains [145–149]. HFF strains were a kind gift of Thomas Stamminger, Erlangen, Germany. The cells were generated as described previously [150].

Supporting Information

S1 Fig. Heatmap plot for Spearman correlation of "overall" gene counts between 8 samples of mouse embryonic fibroblasts (MEF) from the study by [61]. The correlation of 4 IRS-1 replicates is larger then correlation between the 4 wildtype (wt) samples. The notation "2009" and "2010" denoted the re-sequencing of one sample (technical sequencing replicate). These samples exhibit the highest correlation values (mean = 0.997). The notation "l2/l8" and "l4/l1" denote biological replicates. These samples exhibit high correlation values too (mean = 0.990). The correlation between the two conditions (IRS-1 and wt) is lower than between all kind of replicates. This situation is confirmed by the dendrogram.
(TIF)

S2 Fig. Heatmap of Spearman correlation values for 30 fibroblast strains from triplicates derived from one single vial. The colors on the left side encode the different cell lines (red: BJ; blue: HFF; green: IMR-90; violet: MRC-5; orange: WI-38). The colors on top encode the PD (gray: young stage; black: old/senescent stage). Despite the group of senescent IMR-90 samples, largest correlation can be observed between the three replicates for each PD visual by tight grouping in the dendrogram.
(TIF)

S3 Fig. MDS plot revealing the correlation in the mRNA expression pattern at different PDs of MRC-5, HFF, WI-38, BJ and IMR-90 fibroblast strains. The fibroblast strains were maintained in culture as triplicates from young PD till they achieved senescence. The expression pattern reveals the clustering of early PD fibroblasts (triplicates) together and is clearly separated from the triplicate cluster of late PD fibroblasts. This pattern was observed for both HFF and MRC-5 fibroblasts. The plot also reveals a clear separation in the expression pattern between the two fibroblast cell strains.
(TIF)

S4 Fig. Comparison of mean fold change of mRNA expression levels of selected genes derived from real-time PCR and RNA-seq. Mean fold change of mRNA expression levels derived from real-time PCR (A1, B1, C1, D1) and RNA-seq (A2, B2, C2, D2) of selected genes (IGFBP7, CTSK, DKK3, TMEM47, CCND1, ID3, CCNB1 [C'B1], p21, CCNA2 [C'A2], C3, Wnt16 [W'16], IGFBP2 [IGF'2]) most differentially expressed with age in MRC-5 (A1, A2, B1, B2) and HFF strains (C1, C2, D1, D2). Mean fold change values of mRNA expression levels of young PD fibroblasts were normalized to 1 and compared with expression levels of old PD fibroblasts. The

bars indicate the mean ± S.D. Values statistically different from their controls (Student's t-test, 95% confidence level) are indicated with an asterix. * $p < 0.05$, ** $p < 0.01$, *** $p < 0.001$—Significantly different compared to young PD fibroblasts. n = 3. Note: Fig B1, D1, decrease in mRNA expression levels of ID3 with age is significant ($p < 0.01$) when n = 2. Fig C1, increase in mRNA expression levels of IGFBP7 with age is significant ($p < 0.001$) when n = 2. Fig B2, increase in mRNA expression levels of p21 with age is significant ($p < 0.05$) when n = 2.
(TIF)

S5 Fig. The list of significantly up-regulated genes with age in each of the five fibroblast strains (51–100). The red background represents genes commonly up-regulated with age in foreskin fibroblasts (HFF and BJ) and green background reveals genes commonly up-regulated among all the three embryonic lung fibroblasts (MRC-5, IMR-90 and WI-38) as well as between the fibroblasts derived from female donors (IMR-90 and WI-38) among the hundred most differentially regulated genes with age.
(TIF)

S6 Fig. The list of significantly down-regulated genes with age in each of the five fibroblast strains (51–100). The red background represents genes commonly down-regulated with age in foreskin fibroblasts (HFF and BJ) and green background reveals genes commonly down-regulated among all the three embryonic lung fibroblasts (MRC-5, IMR-90 and WI-38) as well as between the fibroblasts derived from female donors (IMR-90 and WI-38) among the hundred most differentially regulated genes with age.
(TIF)

S1 Table. Forward and reverse sequence of the primers. The forward and reverse sequence of the primers designed for selected genes investigated for their mRNA expression levels using real-time PCR.
(TIF)

S2 Table. Common significantly up-regulated genes classified based on origin of the fibroblast strains. List of commonly up-regulated genes with age between foreskin fibroblasts (HFF and BJ), among the embryonic lung fibroblasts (MRC-5, IMR-90 and WI-38) and between each of the embryonic lung fibroblasts among the hundred most differentially regulated genes.
(TIF)

S3 Table. Common significantly up-regulated genes on individual comparison of the foreskin fibroblast strains with embryonic lung fibroblasts. List of commonly up-regulated genes with age between foreskin and embryonic lung fibroblasts (HFF and MRC-5, HFF and IMR-90, HFF and WI-38, BJ and MRC-5, BJ and IMR-90, BJ and WI-38), among the hundred most differentially regulated genes.
(TIF)

S4 Table. Common significantly down-regulated genes classified based on origin of the fibroblast strains. List of commonly down-regulated genes with age between foreskin fibroblasts (HFF and BJ), among the embryonic lung fibroblasts (MRC-5, IMR-90 and WI-38) and between each of the embryonic lung fibroblasts among the hundred most differentially regulated genes.
(TIF)

S5 Table. Common significantly down-regulated genes on individual comparison of the foreskin fibroblast strains with embryonic lung fibroblasts. List of commonly down-regulated genes with age between foreskin and embryonic lung fibroblasts (HFF and MRC-5, HFF and IMR-90, HFF and WI-38, BJ and MRC-5, BJ and IMR-90, BJ and WI-38), among the

hundred most differentially regulated genes.
(TIF)

S6 Table. Pathways most differentially regulated with age in the five fibroblast strains. The list of significantly differentially regulated [up- and down-regulated pathways] with age in each of the five fibroblast strains (A, HFF; B, MRC-5; C, BJ; D, IMR-90; E, WI-38).
(TIF)

Acknowledgments

Author Contributions

Conceived and designed the experiments: SM SD PH. Performed the experiments: SM MB SP JS MG. Analyzed the data: SM MB SP SD. Contributed reagents/materials/analysis tools: SD PH MP RG. Wrote the paper: SM SP MB MG CK RG AC MP SD PH. Read the manuscript and contributed to varying degrees: SM SP MB MG JS CK RG AC MP SD PH.

References

1. Hayflick L, Moorhead P. The serial cultivation of human diploid cell strains. Exp Cell Res. 1961; 25: 585–621. PMID: 13905658

2. Ben-Porath I, Weinberg RA. When cells get stressed: an integrative view of cellular senescence. J Clin Invest. 2004; 113(1): 8–13. PMID: 14702100

3. Munoz-Espin D, Serrano M. Cellular senescence: from physiology to pathology. Nat Rev Mol Cell Biol. 2014; 15: 482–496. doi: 10.1038/nrm3823 PMID: 24954210

4. Rodier F, Campisi J. Four faces of cellular senescence. J Cell Biol. 2011; 192(4): 547–556. doi: 10.1083/jcb.201009094 PMID: 21321098

5. Baker DJ, Childs BG, Durik M, Wijers ME, Sieben CJ, Zhong J, et al. Nature. 2016; 530(7589): 184–189. doi: 10.1038/nature16932 PMID: 26840489

6. Di Leonardo A, Linke SP, Clarkin K, Wahl GM. DNA damage triggers a prolonged p53-dependent G1 arrest and long-term induction of Cip1 in normal human fibroblasts. Genes Dev. 1994; 8(21), 2540–2551. PMID: 7958916

7. Mallette FA, Gaumont-Leclerc MF, Ferbeyre G. The DNA damage signaling pathway is a critical mediator of oncogene-induced senescence. Genes Dev. 2007; 21(1): 43–48. PMID: 17210786

8. Von Zglinicki T, Saretzki G, Ladhoff J, Fagagna FdAd, Jackson SP. Human cell senescence as a DNA damage response. Mech Ageing Dev. 2005; 126(1): 111–117. PMID: 15610769

9. Von Zglinicki T, Saretzki G, Docke W, Lotze C. Mild hyperoxia shortens telomeres and inhibits proliferation of fibroblasts a model for senescence? Exp Cell Res. 1995; 220: 186–193. PMID: 7664835

10. Chen Q, Ames BN. Senescence like growth arrest by hydrogen peroxide in human fibroblast F65 cells. Proc Natl Acad Sci USA. 1994; 91: 4130–4134. PMID: 8183882

11. Serrano M, Lin AW, McCurrach ME, Beach D, Lowe SW. Oncogenic ras Provokes Premature Cell Senescence Associated with Accumulation of p53 and p16INK4a. Cell. 1997; 88(5): 593–602. PMID: 9054499

12. Lin AW, Barradas M, Stone JC, van Aelst L, Serrano M, Lowe SW. Premature senescence involving p53 and p16 is activated in response to constitutive MEK/MAPK mitogenic signaling. Genes Dev. 1998; 12: 3008–3019. PMID: 9765203

13. Zhu J, Woods D, Mcmohan M, Bishop JM. Senescence of human fibroblasts induced by oncogenic Raf. Genes Dev. 1998; 12: 2997–3007. PMID: 9765202

14. Bertram MJ, Berube NG, Hang-Swanson X, Ran Q, Leung JK, Bryce S, et al. Identification of a gene that reverses the immortal phenotype of a subset of cells and is a member of a novel family of transcription factor-like genes. Mol Cell Biol. 1999; 19: 1479–1485. PMID: 9891081

15. Kato JY, Matsuoka M, Polyak K, Massaque J, Sherr CJ. Cyclic AMP induced G1 phase arrest mediated by an inhibitor (p27Kip1) of cyclin dependent kinase 4 activation. Cell. 1994; 79(3): 487–496. PMID: 7954814

16. Dimri GP, Lee X, Basile G, Acosta M, Scott G, Roskelley C, et al. A biomarker that identifies senescent human cells in culture and in aging skin in vivo. Proc Natl Acad Sci USA. 1995; 92(20): 9363–9367. PMID: 7568133

17. Narita M, Nuñez S, Heard E, Narita M, Hearn SA, Spector DL, et al. Cell. 2003; 113(6): 703–716. PMID: 12809602

18. Kuilman TC, Michaloglou C, Mooi WJ, Peeper DS. The essence of senescence. Genes Dev. 2010; 24 (22): 2463–2479. doi: 10.1101/gad.1971610 PMID: 21078816

19. Sikora ET, Arendt T, Bennett M, Narita M. Impact of cellular senescence signature on ageing research. Ageing Res Rev. 2011; 10(1): 146–152. doi: 10.1016/j.arr.2010.10.002 PMID: 20946972

20. Cristofalo VJ, Lorenzini A, Allen RG, Torres C, Tresini M. Replicative senescence: a critical review. Mech Ageing Dev. 2004; 125(10–11): 827–848. PMID: 15541776

21. Herbig U, Jobling WA, Chen BPC, Chen DJ, Sedivy JM. Telomere Shortening Triggers Senescence of Human Cells through a Pathway Involving ATM, p53, and p21CIP1, but Not p16INK4a. Mol Cell. 2004; 14(4): 501–513. PMID: 15149599

22. Jeyapalan JC, Ferreira M, Sedivy JM, Herbig U. Accumulation of senescent cells in mitotic tissue of aging primates. Mech Ageing Dev. 2007; 128(1): 36–44. PMID: 17116315

23. Robles SJ, Adami GR. Agents that cause DNA double strand breaks lead to p16INK4a enrichment and the premature senescence of normal fibroblasts. Oncogene. 1998; 16(9): 1113–1123. PMID: 9528853

24. Ressler S, Bartkova J, Niederegger H, Bartek J, Scharffetter-Kochanek K, Jansen-Dürr P, et al. p16INK4A is a robust in vivo biomarker of cellular aging in human skin. Aging Cell. 2006; 5(5): 379–389. PMID: 16911562

25. Kosar M, Bartkova J, Hubackova S, Hodny Z, Lukas J, Bartek J. Senescence-associated heterochromatin foci are dispensable for cellular senescence, occur in a cell type- and insult-dependent manner and follow expression of p16(ink4a). Cell Cycle. 2011; 10(3): 457–468. PMID: 21248468

26. Cristofalo VJ, Volker C, Francis MK, Tresini M. Age-dependent modifications of gene expression in human fibroblasts. Crt Rev Eukaryot Gene Expr. 1998; 8(1): 43–80.

27. Linskens MH, Feng J, Andrews WH, Enlow BE, Saati SM, Tonkin LA, et al. Cataloging altered gene expression in young and senescent cells using enhanced differential display. Nucleic Acids Res. 1995; 23(16): 3244–3251. PMID: 7667101

28. Shelton DN, Chang E, Whittier PS, Choi D, Funk WD. Microarray analysis of replicative senescence. Curr Biol. 1999; 9(17): 939–945. PMID: 10508581

29. Acosta JC, O'Loghlen A, Banito A, Guijarro MV, Augert A, Raguz S, et al. Chemokine signaling via the CXCR2 receptor reinforces senescence. Cell. 2008; 133(6): 1006–1018. doi: 10.1016/j.cell.2008.03.038 PMID: 18555777

30. Wajapeyee N, Serra RW, Zhu X, Mahalingam M, Green MR. Oncogenic BRAF induces senescence and apoptosis through pathways mediated by the secreted protein IGFBP7. Cell. 2008; 132(3): 363–374. doi: 10.1016/j.cell.2007.12.032 PMID: 18267069

31. Coppé JP, Desprez PY, Krtolica A, Campisi J. The senescence-associated secretory phenotype: the dark side of tumor suppression. Annu Rev Pathol. 2010; 5: 99–118. doi: 10.1146/annurev-pathol-121808-102144 PMID: 20078217

32. Klement K, Melle C, Murzik U, Diekmann S, Norgauer J, Hemmerich P. Accumulation of annexin A5 at the nuclear envelope is a biomarker of cellular aging, Mech Ageing Dev. 2012; 133(7): 508–522. doi: 10.1016/j.mad.2012.06.003 PMID: 22728018

33. Chaturvedi V, Qin JZ, Denning MF, Choubey D, Diaz MO, Nickoloff BJ. Apoptosis in proliferating, senescent, and immortalized keratinocytes. J Biol Chem. 1999; 274(33): 23358–23367. PMID: 10438513

34. Marcotte RL, Lacelle C, Wang E. Senescent fibroblasts resist apoptosis by downregulating caspase-3. Mech Ageing Dev. 2004; 125(10–11): 777–783. PMID: 15541772

35. Marthandan S, Priebe S, Hemmerich P, Klement K, Diekmann S. Long-term quiescent fibroblast cells transit into senescence. PLoS One. 2014; 9: e115597. doi: 10.1371/journal.pone.0115597 PMID: 25531649

36. Smogorzewska A, de Lange T. Different telomere damage signaling pathways in human and mouse cells. EMBO J. 2002; 21(16): 4338–4348. PMID: 12169636

37. Ohtani N, Yamakoshi K, Takahashi A, Hara E. The p16INK4a-RB pathway: molecular link between cellular senescence and tumor suppression. J Med Invest. 2004; 51: 146–153. PMID: 15460900

38. Itahana K, Zou Y, Itahana Y, Martinez JL, Beausejour C, Jacobs JJ, et al. Control of the replicative life span of human fibroblasts by p16 and the polycomb protein Bmi-1. Mol Cell Biol. 2003; 23(1): 389–401. PMID: 12482990

39. d'Adda di Fagagna F, Reaper PM, Clay-Farrace L, Fiegler H, Carr P, Von Zglinicki T, et al. A DNA damage checkpoint response in telomere-initiated senescence. Nature. 2003; 426(6963): 194–198. PMID: 14608368

40. Takai H, Smogorzewska A, de Lange T. DNA damage foci at dysfunctional telomeres. Curr Biol. 2003; 13(17): 1549–1556. PMID: 12956959

41. Nakamura AJ, Redon CE, Bonner WM, Sedelnikova OA. Telomere-dependent and telomere-independent origins of endogenous DNA damage in tumor cells. Aging (Albany NY). 2009; 1(2): 212–218.

42. Gire V, Roux P, Wynford-Thomas D, Brondello JM, Dulic V. DNA damage checkpoint kinase Chk2 triggers replicative senescence. EMBO J. 2004; 23(13): 2554–2563. PMID: 15192702

43. Goodarzi AA, Noon AT, Deckbar D, Ziv Y, Shiloh Y, Löbrich M, et al. ATM signaling facilitates repair of DNA double-strand breaks associated with heterochromatin. Mol Cell. 2008; 31(2): 167–177. doi: 10.1016/j.molcel.2008.05.017 PMID: 18657500

44. Ben-Porath I, Weinberg RA. The signals and pathways activating cellular senescence. Int. J. Biochem. Cell Biol. 2005; 37(5): 961–976. PMID: 15743671

45. Shay JW, Wright WE. Senescence and immortalization: role of telomeres and telomerase. Carcinogenesis. 2005; 26(5): 867–874. PMID: 15471900

46. Cosme-Blanco W, Chang S. Dual roles of telomere dysfunction in initiation and suppression of tumorigenesis. Exp Cell Res. 2008; 314(9): 1973–1979. doi: 10.1016/j.yexcr.2008.03.011 PMID: 18448098

47. Toussaint O, Medrano EE, von Zglinicki T. Cellular and molecular mechanisms of stress-induced premature senescence (SIPS) of human diploid fibroblasts and melanocytes. Exp Gerontol. 2000; 35(8): 927–945. PMID: 11121681

48. Schäuble S, Klement K, Marthandan S, Münch S, Heiland I, Schuster S, et al. Quantitative Model of Cell Cycle Arrest and Cellular Senescence in Primary Human Fibroblasts. Plos One. 2012; 7: e42150. doi: 10.1371/journal.pone.0042150 PMID: 22879912

49. Campisi J, Sedivy J. How does proliferative homeostasis change with age? What causes it and how does it contribute to aging? J Gerontol A Biol Sci Med Sci. 2009; 64(2): 164–166. doi: 10.1093/gerona/gln073 PMID: 19228778

50. Kronschnabl M, Stamminger T. Synergistic induction of intercellular adhesion molecule-1 by the human cytomegalovirus transactivators IE2p86 and pp71 is mediated via an Sp1-binding site. J Gen Virol. 2003; 84(1): 61–73.

51. Honda S, Hjelmeland LM, Handa JT. Oxidative stress–induced single-strand breaks in chromosomal telomeres of human retinal pigment epithelial cells in vitro. Invest Oph- thalmol Vis Sci. 2001; 42: 2139–2144.

52. Sivakumar S, Daum JR, Tipton AR, Rankin S, Gorbsky GJ. The spindle and kinetochore associated (Ska) complex enhances binding of the anaphase promoting complex/cyclosome (APC/C) to chromosomes and promote s mitotic exit. Mol Cell Biol. 2014; 25(5): 594–605.

53. Pfaffl MW, Horgan GW, Dempfle L. Relative expression software tool (REST) for group-wise comparison and statistical analysis of relative expression results in real-time PCR. Nucleic Acids Res. 2002; 30(9): e36. PMID: 11972351

54. Bentley DR, Balasubramanian S, Swerdlow HP, Smith GP, Milton J, Brown CG, et al. Accurate whole human genome sequencing using reversible terminator chemistry. Nature. 2008; 456: 53–59. doi: 10.1038/nature07517 PMID: 18987734

55. Trapnell C, Pachter L, Salzberg SL. TopHat: discovering splice junctions with RNA-Seq. Bioinformatics. 2009; 25(9): 1105–1111. doi: 10.1093/bioinformatics/btp120 PMID: 19289445

56. Flicek P, Amode MR, Barrell D, Beal K, Brent S, Carvalho-Silva D, et al. Ensembl 2012. Nucleic Acids Res. 2012; 40: D84–D90. doi: 10.1093/nar/gkr991 PMID: 22086963

57. R Development Core Team. R: A language and environment for statistical computing. R Foundation for Statistical Computing, Vienna, Austria; 2008. ISBN 3-900051-07-0. Available: http://www.R-project.org.

58. Anders S, Huber W. Differential expression analysis for sequence count data. Genome Biol. 2010; 11: R106. doi: 10.1186/gb-2010-11-10-r106 PMID: 20979621

59. Robinson MD, McCarthy DJ, Smyth GK. edgeR: a Bioconductor package for differential expression analysis of digital gene expression data. Bioinformatics. 2010; 26: 139–140. doi: 10.1093/bioinformatics/btp616 PMID: 19910308

60. Benjamini Y, Hochberg Y. Controlling the false discovery rate: a practical and powerful approach to multiple testing. Journal of the Royal Statistical Society, Series B. 1995; 57(1): 289–300.

61. Zarse K, Schmeisser S, Groth M, Priebe S, Beuster G, Kuhlow D, et al. Impaired insulin/IGF1 signaling extends life span by promoting mitochondrial L-proline catabolism to induce a transient ROS signal. Cell Metab. 2012; 15: 451–465. doi: 10.1016/j.cmet.2012.02.013 PMID: 22482728

62. Barrett T, Wilhite SE, Ledoux P, Evangelista C, Kim IF, Tomashevsky M, et al. NCBI GEO: archive for functional genomics data sets-update. Nucleic Acids Res. 2013; 41: D991–5. doi: 10.1093/nar/gks1193 PMID: 23193258

63. Rustici G, Kolesnikov N, Brandizi M, Burdett T, Dylag M, Emam I, et al. Array Express update-trends in database growth and links to data analysis tools. Nucelic Acids Res. 2013; 41: D987–90.

64. Zhang H, Pan KH, Cohen SN. Senescence-specific gene expression fingerprints reveal cell-type-dependent physical clustering of up-regulated chromosomal loci. Proc Natl Acad Sci USA. 2003; 100 (6): 3251–3256. PMID: 12626749

65. Yoon IK, Kim HK, Kim YK, Song IH, Kim W, Kim S, et al. Exploration of replicative senescence associated genes in human dermal fibroblasts by cDNA microarray technology. Exp Gerontol. 2004; 39(9): 1369–1378. PMID: 15489060

66. Hardy K, Mansfield L, Mackay A, Benvenuti S, Ismail S, Arora P, et al. Transcriptional networks and cellular senescence in human mammary fibroblasts. Mol Biol Cell. 2005; 16(2): 943–953. PMID: 15574883

67. Johung K, Goodwin EC, DiMaio D. Human papillomavirus E7 repression in cervical carcinoma cells initiates a transcriptional cascade driven by the retinoblastoma family, resulting in senescence. J Virol. 2007; 81(5): 2102–2116. PMID: 17182682

68. Binet R, Ythier D, Robles AI, Collado M, Larrieu D, Fonti C, et al. WNT16B is a new marker of cellular senescence that regulates p53 activity and the phosphoinositide 3-kinase/AKT pathway. Cancer Res. 2009; 69(24): 9183–9191. doi: 10.1158/0008-5472.CAN-09-1016 PMID: 19951988

69. Dhahbi JM, Atamna H, Boffelli D, Magis W, Spindler SR, Martin DI. Deep sequencing reveals novel microRNAs and regulation of microRNA expression during cell senescence. PLoS One. 2011; 6(5): e20509. doi: 10.1371/journal.pone.0020509 PMID: 21637828

70. Kim YM, Byun HO, Jee BA, Cho H, Seo YH, Kim YS, et al. Implications of time-series gene expression profiles of replicative senescence. Aging Cell. 2013; 12(4): 622–634. doi: 10.1111/acel.12087 PMID: 23590226

71. Lackner DH, Hayashi MT, Cesare AJ, Karlseder J. A genomics approach identifies senescence-specific gene expression regulation. Aging Cell. 2014; 13(5): 946–950. doi: 10.1111/acel.12234 PMID: 24863242

72. Davis S, Meltzer P. GEOquery: a bridge between the Gene Expression Omnibus (GEO) and BioConductor. Bioinformatics. 2007; 14: 1846–1847.

73. Smyth GK. Limma: Linear models for microarray data. In Gentleman R, Carey V, Dudoit S, Irizarry R and Huber W (eds.), Bioinformatics and Computational Biology Solutions Using R and Bioconductor, Springer, New York; 2005. pp. 397–420.

74. Gautier L, Cope L, Bolstad BM, Irizarry RA. affy—analysis of Affymetrix GeneChip data at the probe level. Bioinformatics. 2004; 20(3): 307–15. PMID: 14960456

75. Luo W, Friedman MS, Shedden K, Hankenson KD, Woolf PJ. GAGE: generally applicable gene set enrichment for pathway analysis. BMC Bioinformatics. 2009; 10: 161. doi: 10.1186/1471-2105-10-161 PMID: 19473525

76. Marthandan S, Priebe S, Baumgart M, Groth M, Cellerino A, Guthke R, et al. Similarities in gene expression profiles during in vitro aging of primary human embryonic lung and foreskin fibroblasts. Biomed Res Int. 2015; 2015: 731938. doi: 10.1155/2015/731938 PMID: 26339636

77. Chen Q, Fischer A, Reagan JD, Yan LJ, Ames BN. Oxidative DNA damage and senescence of human diploid fibroblast cells. Proc Natl Acad Sci USA. 1995; 92(10): 4337–4341. PMID: 7753808

78. Kortlever RM, Higgins PJ, Bernards R. Plasminogen activator inhibitor-1 is a critical downstream target of p53 in the induction of replicative senescence. Nat Cell Biol. 2006; 8(8): 877–884. PMID: 16862142

79. Munro J, Steeghs K, Morrison V, Ireland H, Parkinson EK. Human fibroblast replicative senescence can occur in the absence of extensive cell division and short telomeres. Oncogene. 2001; 20(27): 3541–3552. PMID: 11429701

80. Leek JT, Scharpf RB, Bravo HC, Simcha D, Langmead B, Johnson WE, et al. Tackling the widespread and critical impact of batch effects in high-throughput data. Nat Rev Genet. 2010; 11(10): 733–39. doi: 10.1038/nrg2825 PMID: 20838408

81. Kauffmann A, Huber W. Microarray data quality control improves the detection of differentially expressed genes. Genomics. 2010; 95(3): 138–42. doi: 10.1016/j.ygeno.2010.01.003 PMID: 20079422

82. Noda A, Ning Y, Venable SF, Pereira-Smith OM, Smith JR. Cloning of senescent cell-derived inhibitors of DNA synthesis using an expression screen. Exp Cell Res. 1994; 211(1): 90–98. PMID: 8125163

83. Coppé JP, Patil CK, Rodier F, Sun Y, Muñoz DP, Goldstein J, et al. Senescence-associated secretory phenotypes reveal cell-nonautonomous functions of oncogenic RAS and the p53 tumor suppressor. PLoS Biol. 2008; 6(12): 2853–2868. doi: 10.1371/journal.pbio.0060301 PMID: 19053174

84. Baege AC, Disbrow GL, Schlegel R. IGFBP3, a marker of cellular senescence, Is overexpressed in human papillomavirus-immortalized cervical cells and enhances IGF-1-induced mitogenesis. J Virol. 2004; 78(11): 5720–5727. PMID: 15140969

85. Kim KS, Seu YB, Baek SH, Kim MJ, Kim KJ, Kim JH, et al. Induction of cellular senescence by insulin-like growth factor binding protein-5 through a p53-dependent mechanism. Mol Biol Cell. 2007; 18(11): 4543–4552. PMID: 17804819

86. Hjelmeland LM. Senescence of the retinal pigmented epithelium. Opthalmol Vis Sci. 1999; 40: 1–2.

87. Matsunaga H, Handa JT, Gelfman CM, Hjelmeland LM. The mRNA phenotype of a human RPE cell line at replicative senescence. Mol Vis. 1999; 29(5): 39.

88. Simpson RM, Wells A, Thomas D, Stephens P, Steadman R, Phillips A. Aging fibroblasts resist phenotypic maturation because of impaired hyaluronan-dependent CD44/epidermal growth factor receptor signaling. Am J Pathol. 2010; 176(3): 1215–1228. doi: 10.2353/ajpath.2010.090802 PMID: 20093489

89. Alexander K, Hinds PW. Requirement for p27(KIP1) in retinoblastoma protein-mediated senescence. Mol Cell Biol. 2001; 21(11): 3616–3631. PMID: 11340156

90. Wagner M, Hampel B, Hütter E, Pfister G, Krek W, Zwerschke W, et al. Metabolic stabilization of p27 in senescent fibroblasts correlates with reduced expression of the F-box protein Skp2. Exp Gerontol. 2001; 37(1): 41–55. PMID: 11738146

91. Kim SJ, Lee HW, Gu Kang H, La SH, Ju Choi IL, Ro JY, et al. Ablation of galectin-3 induces p27^{KIP1} dependent pre-mature senescence without oncogenic stress. Cell Death and Differ. 2014; 21: 1769–1779.

92. Sandhu C, Donovan J, Bhattacharya N, Stampfer M, Worland P, Slingerland J. Reduction of Cdc25A contributes to cyclin E1-Cdk2 inhibition at senescence in human mammary epithelial cells. Oncogene. 2000; 19: 5314–5323. PMID: 11103932

93. Alcorta DA, Xiong Y, Phelps D, Hannon G, Beach D, Barrett JC. Involvement of the cyclin-dependent kinase inhibitor p16 (INK4a) in replicative senescence of normal human fibroblasts. Proc Natl Acad Sci USA. 1996; 93(24): 13742–13747. PMID: 8943005

94. Chen JH, Ozanne SE. Deep senescent human fibroblasts show diminished DNA damage foci but retain checkpoint capacity to oxidative stress. FEBS Lett. 2006; 580: 6669–6673. PMID: 17126333

95. Beauséjour CM, Krtolica A, Galimi F, Narita M, Lowe SW, Yaswen F, et al. Reversal of human cellular senescence: roles of the p53 and p16 pathways. EMBO J. 2003; 22(16): 4212–4222. PMID: 12912919

96. Bonifacio LN, Jarstfer MB. MiRNA Profile Associated with Replicative Senescence, Extended Cell Culture, and Ectopic Telomerase Expression in Human Foreskin Fibroblasts. PLoS One. 2010; 5(9): e12519. doi: 10.1371/journal.pone.0012519 PMID: 20824140

97. Chen J, Xu H, Aronow BJ, Jegga AG. Improved human disease candidate gene prioritization using mouse phenotype. BMC Bioinformatics. 2007; 8: 392. PMID: 17939863

98. Baumgart M, Groth M, Priebe S, Savino A, Testa G, Dix A, et al. RNA-seq of the aging brain in the short lived fish N.furzeri–conserved pathways and novel genes associated with neurogenesis. Aging Cell. 2014; 13(6): 965–74. doi: 10.1111/acel.12257 PMID: 25059688

99. Feeney-Burns L, Eldred GE. The fate of the phagosome: conversion to 'age pigment' and impact in human retinal pigment epithelium. Trans Ophthalmol Soc U K. 1983; 103(4): 416–421.

100. Efferth T. Adenosine triphosphate-binding cassette transporter genes in ageing and age-related diseases. Ageing Res Rev. 2003; 2(1): 11–24. PMID: 12437993

101. Fletcher JI, Haber M, Henderson MJ, Norris MD. ABC transporters in cancer: more than just drug efflux pumps. Nat Rev Cancer. 2010; 10(2): 147–56. doi: 10.1038/nrc2789 PMID: 20075923

102. Silva H, Conboy IM. Aging and stem cell renewal. In: StemBook, editor. The Stem Cell Research Community; 2008.

103. Young AR, Narita M. SASP reflects senescence. EMBO Rep. 2009; 10(3): 228–230. doi: 10.1038/embor.2009.22 PMID: 19218920

104. Coppé JP, Patil CK, Rodier F, Krtolica A, Beauséjour CM, Parrinello S, et al. A human-like senescence-associated secretory phenotype is conserved in mouse cells dependent on physiological oxygen. PLoS One. 2010; 5(2): e9188. doi: 10.1371/journal.pone.0009188 PMID: 20169192

105. Millis A.J., Hoyle M., McCue H.M., Martini H., 1992. Differential expression of metalloproteinase and tissue inhibitor of metalloproteinase genes in aged human fibroblasts. Exp Cell Res. 201 (2), 373–379. PMID: 1322316

106. Kang M.K., Kameta A., Shin K.H., Baluda M.A., Kim H.R., Park N.H., 2003. Senescence-associated genes in normal human oral keratinocytes. Exp Cell Res. 287 (2), 272–281. PMID: 12837283

107. Ford CE, Jary E, Ma SS, Nixdorf S, Heinzelmann-Schwarz VA, Ward RL. The Wnt gatekeeper SFRP4 modulates EMT, cell migration and downstream Wnt signaling in serous ovarian cancer cells. PLoS One. 2013; 8(1): e54362. doi: 10.1371/journal.pone.0054362 PMID: 23326605

108. Veeck J, Dahl E. Targeting the Wnt pathway in cancer: the emerging role of Dickkopf-3. Biochim Biophys Acta. 2012; 1825(1): 18–28. doi: 10.1016/j.bbcan.2011.09.003 PMID: 21982838

109. Baylin SB, Ohm JE. Epigenetic gene silencing in cancer—a mechanism for early oncogenic pathway addiction? Nat Rev Cancer. 2006; 6(2): 107–116. PMID: 16491070

110. Warrier S, Bhuvanalakshmi G, Arfuso F, Rajan G, Millward M, Dharmarajan A. Cancer stem-like cells from head and neck cancers are chemosensitized by the Wnt antagonist, sFRP4, by inducing apoptosis, decreasing stemness, drug resistance and epithelial to mesenchymal transition. Cancer Gene Ther. 2014; 21(9): 381–8. doi: 10.1038/cgt.2014.42 PMID: 25104726

111. Zhao S, Fung-Leung WP, Bittner A, Ngo K, Liu X. Comparison of RNA-seq and microarray in transcriptome profiling of activated T cells. PLoS One. 2014; 9 (1):e78644. doi: 10.1371/journal.pone.0078644 PMID: 24454679

112. Coller HA, Sang L, Roberts JM. A New Description of Cellular Quiescence. PLoS Biol. 2006; 4(3): e83. PMID: 16509772

113. Marthandan S, Priebe S, Groth M, Guthke R, Platzer M, Hemmerich P, et al. Hormetic effect of rotenone in primary human fibroblasts. Immun Ageing. 2015; 12:11. doi: 10.1186/s12979-015-0038-8 PMID: 26380578

114. Wang J, Cai Z, Liu J. Microarray analysis for differentially expressed genes of patients undergoing total knee arthroplasty with ischemia preconditioning. J Orthop Surg Res. 2014; 9(1): 133. doi: 10.1186/s13018-014-0133-0 PMID: 25496472

115. Michishita E, Nakabayashi K, Ogino H, Suzuki T, Fujii M, Ayusawa D. DNA topoisomerase inhibitors induce reversible senescence in normal human fibroblasts. Biochem Biophys Res Commun. 1998; 253(3): 667–671. PMID: 9918785

116. Tanaka H, Arakawa H, Yamaguchi T, Shiraishi K, Fukuda S, Matsui K, et al. A ribonucleotide reductase gene involved in a p53-dependent cell-cycle checkpoint for DNA damage. Nature. 2000; 404 (6773): 42–49. PMID: 10716435

117. Chang ZF, Huang DY. Regulation of thymidine kinase expression during cellular senescence. J Biomed Sci. 2001; 8(2): 176–183. PMID: 11287748

118. Matuoka K, Chen KY, Takenawa T. A positive role of phosphatidylinositol 3-kinase in aging phenotype expression in cultured human diploid fibroblasts. Arch Gerontol Geriatr. 2003; 36(3): 203–219. PMID: 12849077

119. Hall PA, Todd CB, Hyland PL, McDade SS, Grabsch H, Dattani M, et al. The septin-binding protein anillin is overexpressed in diverse human tumors. Clin Cancer Res. 2005; 11(19 Pt 1): 6780–6. PMID: 16203764

120. Suzuki C, Daigo Y, Ishikawa N, Kato T, Hayama S, Ito T, et al. ANLN plays a critical role in human lung carcinogenesis through the activation of RHOA and by involvement in the phosphoinositide 3-kinase/AKT pathway. Cancer Res. 2005; 65(24), 11314–11325. PMID: 16357138

121. Hayashi N, Koller E, Fazli L, Gleave ME. Effects of Eg5 knockdown on human prostate cancer xenograft growth and chemosensitivity. Prostate. 2008; 68(12): 1283–1295. doi: 10.1002/pros.20783 PMID: 18512732

122. Kidokoro T, Tanikawa C, Furukawa Y, Katagiri T, Nakamura Y, Matsuda K. CDC20, a potential cancer therapeutic target, is negatively regulated by p53. Oncogene. 2008; 27(11): 1562–1571. PMID: 17873905

123. Loeser RF. Aging and osteoarthritis: the role of chondrocyte senescence and aging changes in the cartilage matrix. Osteoarthritis Cartilage. 2009; 17(8): 971–979. doi: 10.1016/j.joca.2009.03.002 PMID: 19303469

124. Ueki T, Park JH, Nishidate T, Kijima K, Hirata K, Nakamura Y, et al. Ubiquitination and downregulation of BRCA1 by ubiquitin-conjugating enzyme E2T overexpression in human breast cancer cells. Cancer Res. 2009; 69(22): 8752–8760. doi: 10.1158/0008-5472.CAN-09-1809 PMID: 19887602

125. Kikuchi N, Ishii Y, Morishima Y, Yageta Y, Haraguchi N, Itoh K, et al. Nrf2 protects against pulmonary fibrosis by regulating the lung oxidant level and Th1/Th2 balance. Respir Res. 2010; 11: 31. doi: 10.1186/1465-9921-11-31 PMID: 20298567

126. De Felice B, Garbi C, Wilson RR, Santoriello M, Nacca M. Effect of selenocystine on gene expression profiles in human keloid fibroblasts. Genomics. 2011; 97(5): 265–276. doi: 10.1016/j.ygeno.2011.02.009 PMID: 21371550

127. Yoshida Y, Tsunoda T, Doi K, Tanaka Y, Fujimoto T, Machida T, et al. KRAS-mediated up-regulation of RRM2 expression is essential for the proliferation of colorectal cancer cell strains. Anticancer Res. 2011; 31(7): 2535–2539. PMID: 21873171

128. Aguirre-Portolés C, Bird AW, Hyman A, Cañamero M, Pérez de Castro I, Malumbres M. Tpx2 controls spindle integrity, genome stability, and tumor development. Cancer Res. 2012; 72(6): 1518–1528. doi: 10.1158/0008-5472.CAN-11-1971 PMID: 22266221

129. Gasnereau I, Boissan M, Margall-Ducos G, Couchy G, Wendum D, Bourgain-Guglielmetti F, et al. KIF20A mRNA and its product MKlp2 are increased during hepatocyte proliferation and hepatocarcinogenesis. Am J Pathol. 2012; 180(1): 131–140. doi: 10.1016/j.ajpath.2011.09.040 PMID: 22056911

130. Kuo ML, Sy AJ, Xue L, Chi M, Lee MTC, Yen T, et al. RRM2B suppresses the activation of the oxidative stress pathway and is up-regulated by p53 during senescence. Sci Rep. 2012; 2: 822. doi: 10.1038/srep00822 PMID: 23139867

131. Lin Y, Wilson JH. Nucleotide excision repair, mismatch repair, and R-loops modulate convergent transcription-induced cell death and repeat instability. PLoS One. 2012; 7(10): e46807. doi: 10.1371/journal.pone.0046807 PMID: 23056461

132. Pérez de Castro I, Malumbres M. Mitotic Stress and Chromosomal Instability in Cancer: The Case for TPX2. Genes Cancer. 2012; 3(11–12): 721–730. doi: 10.1177/1947601912473306 PMID: 23634259

133. Zuryń A, Litwiniec A, Gackowska L, Pawlik A, Grzanka AA, Grzanka A. Expression of cyclin A, B1 and D1 after induction of cell cycle arrest in the Jurkat cell line exposed to doxorubicin. Cell Biol Int. 2012; 36(12): 1129–1135. doi: 10.1042/CBI20120274 PMID: 22950819

134. Kim N, Song K. KIFC1 is essential for bipolar spindle formation and genomic stability in the primary human fibroblast IMR-90 cell. Cell Struct Funct. 2013; 38(1): 21–30. PMID: 23318213

135. Tao J, Zhi X, Tian Y, Li Z, Zhu Y, Wang W, et al. CEP55 contributes to human gastric carcinoma by regulating cell proliferation. Tumour Biol. 2014; 35(5): 4389–4399. doi: 10.1007/s13277-013-1578-1 PMID: 24390615

136. Wierstra I, Alves J. FOXM1, a typical proliferation-associated transcription factor. Biol Chem. 2007; 388(12): 1257–1274. PMID: 18020943

137. Laoukili J, Kooistra MR, Brás A, Kauw J, Kerkhoven RM, Morrison A, et al. FoxM1 is required for execution of the mitotic programme and chromosome stability. Nat Cell Biol. 2005; 7(2): 126–136. PMID: 15654331

138. Dimri GP, Itahana K, Acosta M, Campisi J. Regulation of a senescence checkpoint response by the E2F1 transcription factor and p14(ARF) tumor suppressor. Mol Cell Biol. 2000; 20(1): 273–285. PMID: 10594030

139. Ors A, Grimaldi M, Kimata Y, Wilkinson CRM, Jones N, Yamano H. Protein synthesis, Post-translational modification and degradation. J Biol Chem. 2009; 284: 23989–23994. doi: 10.1074/jbc.M109.018309 PMID: 19584054

140. Gupta P, Prywes R. ATF1 phosphorylation by the ERK MAPK pathway is required for epidermal growth factor-induced c-jun expression. J Biol Chem. 2002; 277: 50550–50556. PMID: 12414794

141. Bonelli MA, Alfieri RR, Poli M, Petronini PG, Borghetti AF. Heat induced proteasomic degradation of HSF1 in sterum-starved human fibroblasts aging in vitro. Exp Cell Res. 2001; 267: 165–172. PMID: 11426935

142. Meng L, Gabai VL, Sherman MY. Heat shock transcription factor HSF1 plays a critical role in HER2-induced cellular transformation and tumorigenesis. Oncogene. 2010; 29(37): 5204–5213. doi: 10.1038/onc.2010.277 PMID: 20622894

143. Chin JH, Okazaki M, Frazier JS, Hu ZW, Hoffman BB. Impaired cAMP-mediated gene expression and decreased cAMP response element binding protein in senescent cells. Am J Physiol. 1996; 271(1 Pt 1): C362–371. PMID: 8760066

144. Vaughan S, Jat PS. Deciphering the role of nuclear factor-γB in cellular senescence. Aging. 2011; 3: 913–919. PMID: 21990145

145. Holliday R. The commitment of human cells to senescence. Interdiscip Top Gerontol. 2014; 39: 1–7. doi: 10.1159/000358896 PMID: 24862011

146. Jacobs JP, Jones CM, Baille JP. Characteristics of a human diploid cell designated MRC-5. Nature. 1970; 227(5254): 168–170. PMID: 4316953

147. Trlifjová J, Strízová V, Trlifaj L, BudeÆsínský Z, Frühbauer Z. A prolonged cultivation of the human diploid cell strain WI-38. J Hyg Epidemiol Microbiol Immunol. 1968; 12(2): 212–226. PMID: 5752751

148. Friedman HM, Koropchak C. Comparison of WI-38, MRC-5, and IMR-90 cell strains for isolation of viruses from clinical specimens. J Clin Microbiol. 1978; 7(4): 368–371. PMID: 211143

149. Münch S, Weidtkamp-Peters S, Klement K, Grigaravicius P, Monajembashi S, Salomoni P, et al. The tumor suppressor PML specifically accumulates at RPA/Rad51-containing DNA damage repair foci but is nonessential for DNA damage-induced fibroblast senescence. Mol Cell Biol. 2014; 34(10): 1733–1746. doi: 10.1128/MCB.01345-13 PMID: 24615016

150. Tavalai N, Papior P, Rechter S, Leis M, Stamminger T. Evidence for a role of the cellular ND10 protein PML in mediating intrinsic immunity against human cytomegalovirus infections. J Virol. 2006; 80(16): 8006–8018. PMID: 16873257